# Short-Term Interaction between Silent and Devastating Earthquakes in Mexico

Víctor M. Cruz-Atienza[1,1], Josué Tago[2,2], Carlos Villafuerte[1,1], Meng Wei[3,3], Ricardo Garza-Girón[4,4], Luis A. Dominguez[5,5], Vladimir Kostoglodov[1,1], Takuya Nishimura[6,6], Sara Franco[7,7], Jorge Real[1,1], Miguel A. Santoyo[1,1], Yoshihiro Ito[6,6], and Ekaterina Kazachkina[8,8]

[1]Instituto de Geofísica, Universidad Nacional Autónoma de México, Mexico City, Mexico
[2]Facultad de Ingeniería, Universidad Nacional Autónoma de México, Mexico City, Mexico
[3]Graduate School of Oceanography, University of Rhode Island, USA
[4]Department of Earth and Planetary Sciences, University of California, Santa Cruz, USA
[5]Escuela Nacional de Estudios Superiores, Universidad Nacional Autónoma de México, Mexico
[6]Disaster Prevention Research Institute, Kyoto University, Japan
[7]Instituto de Geofísica
[8]Instituto de Geofísica, Universidad Nacional Autónoma de México, Mexico City, Mexico.

November 30, 2022

**Abstract**

Triggering of large earthquakes on a fault that hosts aseismic slip or, conversely, triggering of slow slip events (SSE) by passing seismic waves involves seismological questions with major hazard implications. Just a few observations plausibly suggest that such interactions actually happen in nature. In this study we show that three recent devastating earthquakes in Mexico are likely related to SSEs, describing a cascade of events interacting with each other on a regional scale via quasi-static and/or dynamic perturbations. Such interaction seems to be conditioned by the transient memory of Earth materials subject to the "traumatic" stressing produced by the seismic waves of the great Mw8.2 Tehuantepec earthquake, which strongly disturbed the aseismic beating over a 650 km long segment of the subduction plate interface. Our results imply that seismic hazard in large populated areas is a short-term evolving function of seismotectonic processes that are often observable.

# Short-Term Interaction between Silent and Devastating Earthquakes in Mexico

**Authors:** V. M. Cruz-Atienza[1]*, J. Tago[2], C. Villafuerte[3], M. Wei[4], R. Garza-Girón[5], L. A. Dominguez[6], V. Kostoglodov[1], T. Nishimura[7], S. I. Franco[1], J. Real[1], M. A. Santoyo[1], Y. Ito[7] and E. Kazachkina[3].

**Affiliations**

[1]Instituto de Geofísica, Universidad Nacional Autónoma de México, Mexico City, Mexico.

[2]Facultad de Ingeniería, Universidad Nacional Autónoma de México, Mexico City, Mexico.

[3]Posgrado en Ciencias de la Tierra, Universidad Nacional Autónoma de México, Mexico City, Mexico.

[4]Graduate School of Oceanography, University of Rhode Island, USA.

[5]Department of Earth and Planetary Sciences, University of California, Santa Cruz, USA.

[6]Escuela Nacional de Estudios Superiores, Universidad Nacional Autónoma de México, Mexico.

[7]Disaster Prevention Research Institute, Kyoto University, Japan.

*Correspondence to: cruz@geofisica.unam.mx

**July 2020**

## Abstract

Triggering of large earthquakes on a fault that hosts aseismic slip or, conversely, triggering of slow slip events (SSE) by passing seismic waves involves seismological questions with major hazard implications. Just a few observations plausibly suggest that such interactions actually happen in nature. In this study we show that three recent devastating earthquakes in Mexico are likely related to SSEs, describing a cascade of events interacting with each other on a regional scale via quasi-static and/or dynamic perturbations. Such interaction seems to be conditioned by the transient memory of Earth materials subject to the "traumatic" stressing produced by the seismic waves of the great Mw8.2 Tehuantepec earthquake, which strongly disturbed the aseismic beating over a 650 km long segment of the subduction plate interface. Our results imply that seismic hazard in large populated areas is a short-term evolving function of seismotectonic processes that are often observable.


## Introduction

Seismicity rate varies over time and depends on changes in both the state of stress and properties of the solid Earth. The diversity of earthquakes discovered in recent years, together with new observations of very small transient variations in the crustal properties, offer an unprecedented perspective for exploring causality between different seismotectonic processes. Inferred effects of slow slip events (SSE, also called silent earthquakes) on large and devastating earthquakes have led to critical questions closely related to seismic hazard. The role of SSEs in the seismic cycle has been identified as preponderant in the initiation of some megathrust earthquakes (*1-5*). Observations also show that transient waves from teleseismic or regional earthquakes may trigger SSEs and tectonic tremor (*6-10*), which are two closely related phenomena in active faults. Highly pressurized fluids where slow earthquakes happen (*11*) make frictional conditions very sensitive to small stress or strain perturbations (*12, 13*), thus playing an important role in the generation of slow earthquakes and, certainly, in their interaction with devastating events.

Recently, three major earthquakes took place in southcentral Mexico causing more than 480 deaths and losses for 1,6 billion dollars. The earthquake sequence initiated with the great Mw8.2 Tehuantepec event on September 8, 2017, the largest earthquake ever recorded in Mexico, which may have broken the whole subducted Cocos lithosphere (*14, 15*) (Fig. 1). Eleven days later and 480 km northwest, on September 19, the Mw7.1 Puebla-Morelos normal-faulting (57 km depth) event delivered a deadly shock to Mexico City (*16*), where 44 buildings collapsed and 600 where seriously damaged despite its remarkably slow, dissipative rupture (*17*). The sequence ended five months later on February 16, 2018, with a Mw7.2 thrust event below Pinotepa Nacional, Oaxaca (hereafter Pinotepa), more than 250 km away from both previous earthquakes, causing damage where similar ruptures have severely harmed local infrastructures in the past. Besides damaging earthquakes, the Mexican subduction zone is prone to very large SSEs and persistent tectonic tremor, especially in the Guerrero and Oaxaca states, which extend along the epicentral regions of the earthquake sequence (*18-23*). At the time of the Tehuantepec and Puebla-Morelos events, two separate SSEs were taking place in Guerrero and Oaxaca (*23, 24*). As we shall see, other SSEs also happened in both states in an unusual way during and after the five-month earthquake sequence, featuring a unique and fascinating story that deserves to be told and understood. In this work we investigate possible interactions between such SSEs and the three devastating earthquakes, and found that most of our observations can be explained as a regional cascade of causally related events through short-term, quasi-static and dynamic interactions that have strongly perturbed the regional plate-interface aseismic beating.

## Results

- **Plate Interface Aseismic Slip History**

In the Mexican subduction zone, slow surface displacement can be explained in terms of the aseismic slip between the subducted Cocos plate and the overriding North American plate. Such slip can be understood either as SSEs, post-seismic relaxations or plate interface coupling (PIC, i.e. $1 - v / b$, where $v$ is the interplate slip rate, $b$ is the plate convergence rate and $v \leq b$). For imaging the spatial evolution of the aseismic slip in those terms, we inverted continuous displacement records at 57 permanent GPS stations from November 2016 to October 2019, the largest dataset ever analyzed in Mexico, making use of ELADIN, a recently developed and powerful technique (*25*) (Methods, Fig. S1). Careful examination of the GPS time series revealed several transient deformations in the Guerrero and Oaxaca states. Figure 2 presents the aseismic-slip inversion results for the whole analyzed period, where we find: (Fig. 2B) the 2017 Mw6.9 Guerrero SSE that reached shallow interface regions (up to 10 km depth, Fig. S2) and the initiation of the 2017 Mw6.9 Oaxaca SSE before the onset of the earthquake sequence; (Fig. 2B-2D) the evolution of the 2017 Mw6.9 Oaxaca SSE; (Fig. 2E-2F) the Mw7.2 post-seismic slip of the Pinotepa earthquake that lasted at least until November 2018, together with a neighboring but separated, 200 km length, Mw6.9 SSE in Guerrero (second one); and (Fig. 2G-2H) the concomitant evolution of the 2019 Mw7.0 Guerrero (third one) and Mw6.9 Oaxaca (second one) SSEs (Table 1). The aseismic slip evolution for all analyzed windows is summarized in Figs. 1 and S2. Considering only the slip areas encompassed by 1 cm contours (Fig. 1), the aseismic moment released during this three-year period is equivalent to a magnitude Mw7.5 earthquake ($M_0$ = 2.32 x $10^{20}$ Nw*m), where only 31% of $M_0$ corresponds to the post-seismic slip of the Mw7.2 Pinotepa rupture (Table 1).

Figure 3 shows the aseismic slip evolution (for events with Mw > 6) throughout the period of the earthquake sequence. For the analysis, we separated the slip history in two parts; one before (Fig. 3A) and the other after (Fig. 3B) the Pinotepa earthquake. The second part includes the previous inverted window as a reference. Panel A shows that the 2017 Guerrero SSE basically ended with the occurrence of the devastating Tehuantepec and Puebla-Morelos earthquakes. Only a few minor slip patches were imaged in the following three months (Fig. 2C). We further see that the 2017 Oaxaca SSE, which also initiated months before the earthquakes, developed bilaterally during the five months that followed. More interestingly, examination of the GPS time series in the southern stations reveals a sudden reversal of the displacement direction from north to south (green circles, left) at the moment of the great Tehuantepec event. In contrast, northern stations (green circles, right) feature a slow, typical SSE initiation well before, around May-June 2017. The sharp change of the deformation regime in the south suggests that the Tehuantepec earthquake modified the ongoing Oaxaca SSE. In addition, the question arises as to whether the Guerrero and Oaxaca SSEs could have promoted the rupture of the Puebla-Morelos and Pinotepa earthquakes, respectively, as proposed for other earthquakes in Mexico (*5, 21*).

The GPS displacements in Panel B show a similar effect over the ongoing Oaxaca SSE to that inferred for the Tehuantepec earthquake, but in this case produced by the Mw7.2 Pinotepa event. While displacements in the eastern stations show either an ongoing or a smooth, spontaneously initiated SSE before this earthquake (green circles, right), some stations to the west exhibit again an abrupt change of displacements from north to south, right when the earthquake happened (green circles, left).

All reported SSEs (i.e. three in Guerrero and two in Oaxaca) and the post-seismic slip of the Pinotepa earthquake overlap one another outlining a 650 km long, trench-parallel band of aseismic stress release (Fig. 1). Effects of the earthquakes on the SSE activity or, inversely, of the SSEs on the earthquakes' initiation may have occurred due to static and/or dynamic stress/strain perturbations. In the following we examine these possibilities.

- **Stress Transfer and Seismicity**

Stress transfer to active faults has long been recognized as a preponderant factor in earthquake occurrence (*26*). Although fault failure depends on the absolute stress level, changes of the Coulomb Failure Stress (CFS) explain remarkably well rupture sequences and seismicity-rate variations. CFS changes smaller than 50 kPa (0.5 bar) are often spatially well correlated (above 65%) with triggered seismicity and significantly larger (one order of magnitude) than values required for triggering slow earthquakes in subduction zones (*27*).

The 1 cm slip contour of the 2017 Guerrero SSE stopped about 80 km from the Puebla-Morelos intraslab earthquake hypocenter (Fig. 2A). The CFS on the seismogenic fault (i.e. within a 20 km radius from the hypocenter) due to the plate-interface aseismic slip evolution (SSE + PIC) reveals a rise of 50 kPa (0.5 bar) around the earthquake hypocenter in the 40 days preceding the rupture (Fig. S3E, Methods). Albeit this increment is in the upper limit of the 0.1-0.5 bar earthquake triggering threshold commonly referred in the literature (*26*) and similar to the one believed to have triggered the Mw7.3 (2014) Papanoa earthquake by a SSE in Guerrero (*5*), interestingly, it occurred in the last stage of the SSE, when the PIC near the rupture area experienced a recovery, certainly affected by the evolution of the neighboring SSE. As discussed latter, the strong shaking produced in the seismogenic fault by the great Tehuantepec earthquake 11 days earlier, could significantly reduce the intraslab frictional strength and thus assist the Mw7.1 Puebla-Morelos rupture initiation (*28*) driven by the CFS induced by the aseismic slip at the plate interface. To our knowledge, this is the first evidence that an SSE could initiate a devastating intraslab rupture such as the Puebla-Morelos earthquake.

Five months later, the Mw7.2 Pinotepa thrust earthquake took place at the Cocos – North American plate boundary (Fig. 1) while the 2017 Oaxaca SSE was unfolding (Fig. 3A). The detailed aseismic slip and CFS evolution on the plate interface preceding the earthquake is shown in Fig. S4. Around the hypocentral region there is a clear rise of CFS reaching cumulative values close to 400 kPa (4 bar) (Fig. 4A). During the five months following the Mw8.2 Tehuantepec rupture and within a radius of 20 km from the Pinotepa earthquake hypocenter, the CFS experienced a sustained growth of 200 kPa (2 bar) due to the SSE development to the north (Fig. 4B). During the same period, GPS inversions show that the interplate slip rate, which always remained in a coupling regime (i.e. smaller than the plate convergence rate), decreased until the initiation of the earthquake (i.e. the PIC increased from 0.1-0.2 up to ~0.65). To better elucidate the mechanical process leading to the Pinotepa earthquake nucleation, we carefully analyzed the seismicity in the hypocentral region during the year preceding the event using two complementary template matching techniques (Methods, Figs. S5 and S6). Figure 4C shows 21-days event counts with magnitude larger than 2.1 and foci within a 30 km radius from the hypocenter. Our seismic catalog has 431% more detections (5,977 earthquakes) than those reported by the Servicio Sismológico Nacional (SSN) above the completeness magnitudes for the same period and hypocentral distance. One clear feature stands out: seismicity raised steadily after the Mw8.2 Tehuantepec event until the Mw7.2 Pinotepa earthquake, especially during the two previous months (up to ~50% increase), when the Oaxaca SSE induced the largest CFS increment in the hypocentral region (see also Fig. S4F).

The increase in CFS, PIC and seismicity rate in the hypocentral region before the Pinotepa earthquake strongly suggests that the dominant mechanism that led to the onset of rupture corresponds to an asperity model; i.e. a heterogeneous initial stress in the source region was loaded at a mesoscale by the development of the SSE to the north until an overloaded nucleation patch, the asperity (e.g. subducted seamount), overcame the plate interface strength. Notice the outstanding correlation between the CFS concentration and the location of the precursor seismicity next to the earthquake hypocenter (Fig. 4A). Despite the increasing coupling of the plate interface (and CFS) during the preparedness of the earthquake, seismicity also increased. This scenario disfavors the putative widespread idea of a SSE-induced aseismic slip acceleration around the nucleation patch, observed for other large earthquakes (*1, 2*), as the main triggering mechanism for this event. The small magnitude precursor seismicity reveals small-scale processes that escape to our GPS inversions. However, this activity can be explained by a cascading rupture of small, neighboring asperities loaded by the mesoscale effect of the SSE evolution north of the hypocenter.

In addition, except for the large post-seismic slip of the Pinotepa earthquake and the very east portion of the 2017 Oaxaca SSE (Figs. 5B and 5D), static CFS perturbations produced by the earthquake sequence seems not to have had major bearing on the SSE activity.

- **Plate Interface Dynamic Perturbations**

Abrupt changes in the slow crustal deformation pattern after the Tehuantepec and Pinotepa earthquakes (Fig. 3) suggest an effect of both events on the interplate aseismic slip that cannot be explained by static stress transfers, as shown in the last section. However, dynamic stress or strain perturbations produced by seismic waves may have important implications in the elastic properties of fault zone materials (e.g., transient reduction of the bulk modulus) and the slip behavior, especially where slow earthquakes take place (*6, 7, 9, 28-30*). For instance, long-period surface waves from the 2010 Mw8.8 Maule earthquake triggered deep tremor in Guerrero and likely reactivated an ongoing SSE (*8*).

We estimated dynamic perturbations at the plate interface for both earthquakes of the sequence (Methods). Figure 5A shows the CFS peak values produced by the Rayleigh waves of the Mw8.2 Tehuantepec event (Fig. S7) beneath strong motion stations in south-central Mexico. Dynamic perturbations around the 2017 Oaxaca SSE region lasted about 80 s and are characterized by three major wave cycles with CFS values ranging between 75 and 200 kPa, and absolute dilations between $1.4 \times 10^{-6}$ and $6.0 \times 10^{-6}$ (Fig. S8). Albeit the dynamic triggering of slow earthquakes also depends on the (uncertain) preexistent fault condition, dynamic dilations from the Tehuantepec event are two orders of magnitude larger than those produced in Japan by the great Sumatra-Andaman 2004 earthquake, which triggered widespread tremor in Shikoku and Tokai regions (*6*) and CFSs about eight times larger (*31*). The earthquake triggered tremor in Oaxaca (*23*) and a SSE in the San Andreas fault (*10*), 3,000 km northwest from the source. Since the 2017 Oaxaca SSE initiated before the earthquake and considering that tremor sensitivity increases as the slow slip develops (*32*), it is plausible that such dynamic perturbations were responsible of the large SSE enhancement and thus of the sudden change of the crustal deformation pattern in the region (Fig. 3A).

Given that the Mw7.2 Pinotepa earthquake is a much smaller event that occurred closer to the (presumably) triggered 2018 Guerrero SSE (Figs. 2B and 3B), shorter-period body waves could also affect the SSE that was unfolding in Oaxaca at the moment of rupture. Figure 5C shows the complete-wavefield CFS maximum values simulated on the plate interface for the earthquake using the DGCrack numerical platform (*33*) (Methods, Fig. S9). Values range between 100 and 150 kPa within the 2018 Guerrero SSE slip area, and overcome 400 kPa in the post-seismic slip region downdip from the epicenter. In contrast, the co-seismic static CFS change produced by the earthquake is at least two orders of magnitude smaller in the same SSE region (Fig. 5D). This indicates that seismic waves of the Pinotepa earthquake could also be responsible for triggering the second SSE in Guerrero and therefore the change in the regional deformation pattern at the time of the event (Fig. 3B).

- **Mechanics of SSEs Dynamic Triggering**

To assess whether seismic waves from the Tehuantepec and Pinotepa earthquakes could explain the abrupt changes of the crustal deformation pattern, we conducted numerical simulations of SSEs in the framework of rate-and-state (R&S) friction models subject to the stress dynamic perturbations estimated for both earthquakes. Previous studies with similar methods (*10, 34*) focused on dynamically triggered SSEs when the perturbation occurs in the inter-SSE period. However, the Tehuantepec and Pinotepa earthquakes happened during a large SSE in Oaxaca (Fig. 3), making this a unique opportunity to understand the mechanics of SSEs when seismic waves from M7+ and larger regional earthquakes perturb them in a tectonic environment where both phenomena are frequent.

Following Wei et al. (*34*), we developed a 2D R&S SSE model for the Oaxaca region (Fig. 6A) (Methods, Fig. S10). Figure 6C shows the model response to dynamic stresses estimated for the Tehuantepec earthquake at the plate interface under station YOIG, which is located above the 2018

Oaxaca SSE slip area (Figs. 5A and S8). Final slip due to the stress perturbation is about twice the value of the reference, spontaneous SSE (Fig. 6C). Figure 6B shows the "aseismic slip jump" induced by this perturbation, where the propagation speed of the SSE front experiences an abrupt acceleration which, in turn, implies a change of the same order in the surface displacements. The higher the CFS peak value, the larger are both the final slip and the SSE front and slip accelerations (Fig. 6C). The same happens with the perturbations estimated for the Pinotepa earthquake (Fig. 6D). However, despite that peak values over the 2017 Oaxaca SSE region are significantly larger than those induced by Rayleigh waves from the Tehuantepec event (> 250 kPa), they overcome the SSE triggering threshold for a much shorter time (intense phase durations for the Mw8.2 and Mw7.2 events are ~75 s and ~13 s, respectively). Consequently, the slip increment associated with each wavelet exceeding the threshold is smaller. This is clear in the insets of Figures 6C and 6D, where the slip rate response and cumulative slip increment due to several waves from the Pinotepa earthquake is comparable to the increment of a single phase of the Tehuantepec event. Thus, the dominant period of seismic waves also controls its SSE triggering potential and thus the effective fault response (Fig. S10D). Since our model considers only along-dip SSEs propagation and the actual slip in Oaxaca and Guerrero migrated predominantly along-strike, it is clear that seismic waves from both earthquakes could produce a much longer SSE evolution than theoretically predicted by our simple model, explaining thus the observed crustal rebounds initiated with both ruptures (Fig. 3).

## Discussion

During two years, between June 2017 and July 2019, in addition to the devastating earthquake sequence, five large SSEs (Mw > 6.9) occurred in southcentral Mexico over a trench-parallel continuous band of 650 km in length with a cumulative moment magnitude Mw7.4 (Fig. 1, Table 1). Three of them in Guerrero, and the other two in Oaxaca interspersed by the Pinotepa earthquake post-seismic slip with Mw7.2. Among all aseismic events, only the 2017 Guerrero and Oaxaca SSEs initiated before the earthquake sequence, so that 87% of the total aseismic moment was released during the 1.7 years following the great Mw8.2 Tehuantepec rupture, when the earthquake sequence started. Although the three Guerrero SSEs nucleated in different regions (Fig. 2), all of them overlap downdip of the Northwest Guerrero seismic gap with a slip larger than 6 cm each (Figs. 1, 2 and S2). Unlike the last 20 years, during which all SSEs occurred every ~4 years in Guerrero (six events between 1998 and 2017) (*5*), the last two events reported here had much smaller recurrence periods, of 0.25 and 0.5 years for the 2018 and 2019 SSEs, respectively. In Oaxaca something unusual also happened; the plate interface slipped (aseismically) continuously for the whole two years period with at least two reactivations, one during the post-seismic relaxation of the Mw7.2 Pinotepa earthquake, and the other one around November 2018, when the second Oaxaca SSE initiated. Similar M7+ thrust earthquakes had occurred in Oaxaca and Guerrero (*5, 21*), but none was followed by a SSE in the last stage of their post-seismic relaxation. All these observations strongly suggest that, in addition to the dynamic effect of the seismic waves from the Tehuantepec and Pinotepa earthquakes on the ongoing SSEs, the elastic and frictional properties of the plate interface across the entire Mexican subduction zone underwent a transient change due to the extremely large, unprecedented ground shaking on September 8, 2017.

When seismic waves exceed a certain strain threshold, fault gouge materials undergo abnormal non-linear changes that can bring them to a metastable state facilitating the triggering of earthquake and SSEs (*28-30*). Although no mechanical changes have yet been observed in the properties of the plate-interface fault-zone due to strong shaking, large seismic waves can affect the continental crust down to its root for several years (*35*). It is thus reasonable that the Mw8.2 Tehuantepec earthquake is responsible for the extraordinary disruption of the SSE cycle observed at the regional scale, and even for facilitating the dynamic triggering of the SSEs that we report here. The same hypothesis is valid for the Puebla-Morelos and Pinotepa earthquakes, triggered by the 2017 Guerrero and Oaxaca SSEs, respectively, where the loss of fault zone rigidity on both seismogenic faults could occur on September 8 (2017) assisting their rupture initiation (*28*). Therefore, continuous monitoring of the regional deformation and seismic properties of the crust is essential to assess the possibility of future large earthquakes and thus to have a clearer picture of the temporal evolution of the seismic hazard in subduction zones.

# References

1. A. Kato *et al.*, Propagation of slow slip leading up to the 2011 M(w) 9.0 Tohoku-Oki earthquake. *Science* **335**, 705-708 (2012).
2. S. Ruiz *et al.*, Intense foreshocks and a slow slip event preceded the 2014 Iquique Mw 8.1 earthquake. *Science* **345**, 1165-1169 (2014).
3. K. Obara, A. Kato, Connecting slow earthquakes to huge earthquakes. *Science* **353**, 253-257 (2016).
4. N. Uchida, T. Iinuma, R. M. Nadeau, R. Bürgmann, R. Hino, Periodic slow slip triggers megathrust zone earthquakes in northeastern Japan. *Science* **351**, 488-492 (2016).
5. M. Radiguet *et al.*, Triggering of the 2014 Mw7.3 Papanoa earthquake by a slow slip event in Guerrero, Mexico. *Nature Geoscience* **9**, 829-833 (2016).
6. M. Miyazawa, J. Mori, Evidence suggesting fluid flow beneath Japan due to periodic seismic triggering from the 2004 Sumatra-Andaman earthquake. *Geophys. Res. Lett.* **33**, (2006).
7. J. L. Rubinstein *et al.*, Seismic wave triggering of nonvolcanic tremor, episodic tremor and slip, and earthquakes on Vancouver Island. *J. Geophys. Res.* **114**, (2009).
8. D. Zigone *et al.*, Triggering of tremors and slow slip event in Guerrero, Mexico, by the 2010 Mw 8.8 Maule, Chile, earthquake. *Journal of Geophysical Research: Solid Earth* **117**, B09304 (2012).
9. L. M. Wallace *et al.*, Large-scale dynamic triggering of shallow slow slip enhanced by overlying sedimentary wedge. *Nature Geoscience* **10**, 765-770 (2017).
10. E. Tymofyeyeva *et al.*, Slow Slip Event On the Southern San Andreas Fault Triggered by the 2017 Mw8.2 Chiapas (Mexico) Earthquake. *Journal of Geophysical Research: Solid Earth* **124**, 9956-9975 (2019).

11. P. Audet, Y. Kim, Teleseismic constraints on the geological environment of deep episodic slow earthquakes in subduction zone forearcs: A review. *Tectonophysics* **670**, 1-15 (2016).
12. V. M. Cruz-Atienza, C. Villafuerte, H. S. Bhat, Rapid tremor migration and pore-pressure waves in subduction zones. *Nat Commun* **9**, 2900 (2018).
13. E. Warren-Smith *et al.*, Episodic stress and fluid pressure cycling in subducting oceanic crust during slow slip. *Nature Geoscience* **12**, 475-481 (2019).
14. D. Melgar *et al.*, Deep embrittlement and complete rupture of the lithosphere during the Mw 8.2 Tehuantepec earthquake. *Nature Geoscience* **11**, 955-960 (2018).
15. G. Suárez *et al.*, Large scale lithospheric detachment of the downgoing Cocos plate: The 8 September 2017 earthquake (Mw 8.2). *Earth Planet Sc Lett* **509**, 9-14 (2019).
16. S. K. Singh *et al.*, Deadly Intraslab Mexico Earthquake of 19 September 2017 (Mw 7.1): Ground Motion and Damage Pattern in Mexico City. *Seismological Research Letters* **89**, 2193-2203 (2018).
17. A. Mirwald *et al.*, The 19 September 2017 (Mw7.1) Intermediate-Depth Mexican Earthquake: A Slow and Energetically Inefficient Deadly Shock. *Geophys Res Lett* **46**, 2054-2064 (2019).
18. V. Kostoglodov *et al.*, A large silent earthquake in the Guerrero seismic gap, Mexico. *Geophys Res Lett* **30**, (2003).
19. M. Radiguet *et al.*, Slow slip events and strain accumulation in the Guerrero gap, Mexico. *J. Geophys. Res.* **117**, B04305 (2012).
20. C. Villafuerte, V. M. Cruz-Atienza, Insights into the Causal Relationship between Slow Slip and Tectonic Tremor in Guerrero, Mexico. *J Geophys Res* **122**, (2017).
21. S. Graham *et al.*, Slow Slip History for the MEXICO Subduction Zone: 2005 Through 2011. *Pure and Applied Geophysics* **173**, 3445-3465 (2016).

22. J. Maury, S. Ide, V. M. Cruz-Atienza, V. Kostoglodov, Spatiotemporal Variations in Slow Earthquakes Along the Mexican Subduction Zone. *Journal of Geophysical Research: Solid Earth* **123**, 1559-1575 (2018).

23. A. Husker *et al.*, Characteristic Tectonic Tremor Activity Observed Over Multiple Slow Slip Cycles in the Mexican Subduction Zone. *Journal of Geophysical Research: Solid Earth* **124**, 599-608 (2019).

24. V. M. Cruz-Atienza *et al.*, A Seismogeodetic Amphibious Network in the Guerrero Seismic Gap, Mexico. *Seismological Research Letters* **89**, 1435-1449 (2018).

25. J. Tago *et al.*, Adjoint Slip Inversion under a Constrained Optimization Framework: Revisiting the 2006 Guerrero Slow Slip Event. *Earth and Space Science Open Archive*, (2020).

26. R. S. Stein, The role of stress transfer in earthquake occurrence. *Nature* **402**, 605-609 (1999).

27. R. Nakata, N. Suda, H. Tsuruoka, Non-volcanic tremor resulting from the combined effect of Earth tides and slow slip events. *Nature Geoscience* **1**, 676-678 (2008).

28. P. A. Johnson, X. Jia, Nonlinear dynamics, granular media and dynamic earthquake triggering. *Nature* **437**, 871-874 (2005).

29. P. A. Johnson *et al.*, Nonlinear dynamical triggering of slow slip on simulated earthquake faults with implications to Earth. *Journal of Geophysical Research: Solid Earth* **117**, (2012).

30. A. A. Delorey, K. Chao, K. Obara, P. A. Johnson, Cascading elastic perturbation in Japan due to the 2012 Mw8.6 Indian Ocean earthquake. *Science Advances* **1**, e1500468 (2015).

31. M. Miyazawa, E. E. Brodsky, Deep low-frequency tremor that correlates with passing surface waves. *J. Geophys. Res.* **113**, (2008).

32. H. Houston, Low friction and fault weakening revealed by rising sensitivity of tremor to tidal stress. *Nature Geosci* **8**, 409-415 (2015).

33. J. Tago, V. M. Cruz-Atienza, J. Virieux, V. Etienne, F. J. Sánchez-Sesma, A 3D hp-adaptive discontinuous Galerkin method for modeling earthquake dynamics. *Journal of Geophysical Research: Solid Earth* **117**, (2012).

34. M. Wei, Y. Kaneko, P. Shi, Y. Liu, Numerical Modeling of Dynamically Triggered Shallow Slow Slip Events in New Zealand by the 2016 Mw 7.8 Kaikoura Earthquake. *Geophys Res Lett* **45**, 4764-4772 (2018).

35. Q.-Y. Wang *et al.*, Evidence of Changes of Seismic Properties in the Entire Crust Beneath Japan After the Mw 9.0, 2011 Tohoku-oki Earthquake. *Journal of Geophysical Research: Solid Earth* **124**, 8924-8941 (2019).

36. L. Ferrari, T. Orozco-Esquivel, V. Manea, M. Manea, The dynamic history of the Trans-Mexican Volcanic Belt and the Mexico subduction zone. *Tectonophysics* **522**, 122-149 (2012).

37. J. A. Arzate-Flores, R. Molina-Garza, F. Corbo-Camargo, V. Márquez-Ramírez, Low Angle Contact Between the Oaxaca and Juárez Terranes Deduced From Magnetotelluric Data. *Pure and Applied Geophysics* **173**, 3357-3371 (2016).

38. M. Rodríguez-Domínguez, X. Pérez-Campos, C. Montealegre-Cázares, R. W. Clayton, E. Cabral-Cano, Crustal structure variations in south-central Mexico from receiver functions. *Geophys J Int* **219**, 2174-2186 (2019).

39. M. Campillo, S. K. Singh, N. Shapiro, J. Pacheco, R. B. Hermann, Crustal structure south of the Mexican volcanic belt, base on group velocity dispersion. *Geofis Int* **35**, 361-370 (1996).

40. C. DeMets, R. G. Gordon, D. F. Argus, Geologically current plate motions. *Geophys J Int* **181**, 1-80 (2010).

41. E. Cabral-Cano *et al.*, TLALOCNet: A Continuous GPS-Met Backbone in Mexico for Seismotectonic and Atmospheric Research. *Seismological Research Letters* **89**, 373-381 (2018).

42. K. Lagler, M. Schindelegger, J. Böhm, H. Krásná, T. Nilsson, GPT2: Empirical slant delay model for radio space geodetic techniques. *Geophys Res Lett* **40**, 1069-1073 (2013).

43. T. A. Herring, R. W. King, M. A. Floyd, S. C. McClusky, GPS Analysis at MIT. *GAMIT Reference Manual*, (2018).

44. M. Liu, H. Li, M. Zhang, T. Wang, Graphics Processing Unit-Based Match and Locate (GPU-M&L): An Improved Match and Locate Method and Its Application. *Seismological Research Letters* **91**, 1019-1029 (2020).

45. C. J. Chamberlain *et al.*, EQcorrscan: Repeating and Near-Repeating Earthquake Detection and Analysis in Python. *Seismological Research Letters* **89**, 173-181 (2017).

46. R. Garza-Giron, E. Brodsky, Z. Spica, M. Haney, Clog and Crack: Opening and Closing Behavior During a Sustained Explosive Eruption as recorded by its Hidden Earthquakes. *Earth and Space Science Open Archive*, (2020).

47. Z. Spica *et al.*, 3-D shear wave velocity model of Mexico and South US: bridging seismic networks with ambient noise cross-correlations (C1) and correlation of coda of correlations (C3). *Geophys J Int* **206**, 1795-1813 (2016).

48. N. Pulido *et al.*, Scenario Source Models and Strong Ground Motion for Future Mega-earthquakes: Application to Lima, Central Peru. *B Seismol Soc Am* **105**, 368-386 (2015).

## Acknowledgments

We especially thank Yoshihiro Kaneko and Yajing Liu for fruitful discussions to set the R&S fault model, Mathilde Radiguet for discussions on the SSEs inversion, the Servicio Sismológico Nacional of UNAM for providing GPS, strong motion and broadband data, and the Instituto de Ingeniería of UNAM for providing strong motion data. SSE inversions and earthquake numerical simulations were performed in the Gaia and Miztli supercomputing platforms. **Funding:** This work was supported by UNAM-PAPIIT grants IN113814 and IG100617, UNAM-DGTIC grant LANCAD-312, JICA-JST SATREPS-UNAM grant 15543611, CONACyT grants 6471, 255308 and PN15-639, US NSF grant 1654416, AMEXCID-SRE and the Ministry of Civil Protection of the State of Guerrero, Mexico. **Author contributions:** V.M.C.-A. conceived and led the study, performed the GPS inversions, estimated the Mw8.2 dynamic CFSs and wrote the manuscript. J.T. developed the ELADIN inversion method for the study. C.V. estimated the static CFSs, performed the DGCrack simulations and developed processing and visualization tools. M.W. developed and analyzed the SSE R&S models. R.G.G. and L.A.D. performed and analyzed the template-matching seismicity detections. V.K. and T.N. contributed with the GPS data analysis. S.I.F., J.R. and E.K. processed the GPS data and maintained the SATREPS-UNAM GPS stations. M.A.S. participated in the single-station dynamic CFS validation. V.M.C.-A. and Y.I. are the PIs of the SATREPS-UNAM project. All authors reviewed and edited the manuscript. **Competing interests:** Authors declare no competing interests. **Data and materials availability:** GPS and strong motion data from SSN are subject to restriction policies while broadband data is open access (see www.ssn.unam.mx). Strong motion data from I. de I. UNAM are available upon request (see www.uis.unam.mx). SATREPS-UNAM GPS data has restriction policies until March 2025. Methods and codes are available upon request.

**Supplementary Materials**

Methods

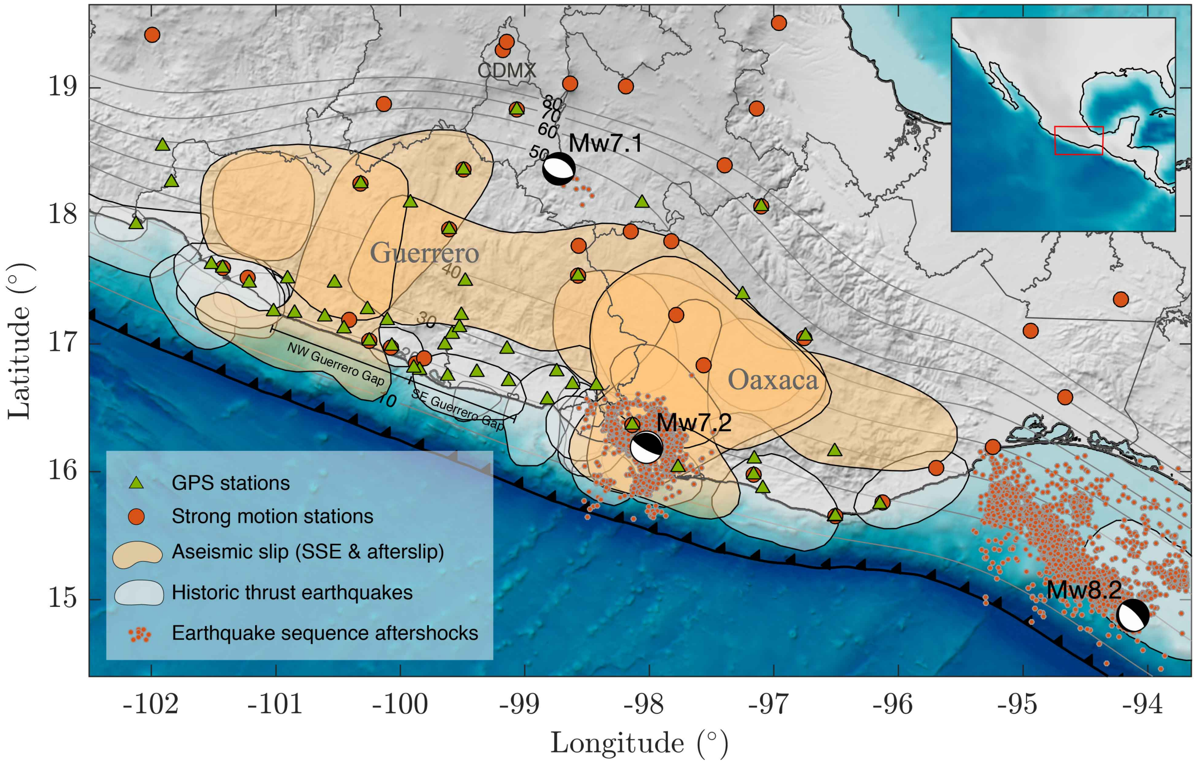


**Fig. 1.** Study region and instrumentation where the Tehuantepec (Mw8.2), Puebla-Morelos (Mw7.1) and Pinotepa (Mw7.2) earthquake sequence took place. Orange shaded areas depict the 1 cm aseismic slip contours imaged between June 2017 and July 2019 in the plate interface (gray contours). White shaded contours depict rupture areas of historic thrust earthquakes. Orange dots show the 10-days aftershock sequences as reported by the SSN except for the Mw7.1 earthquake, for which three-months aftershocks are reported.

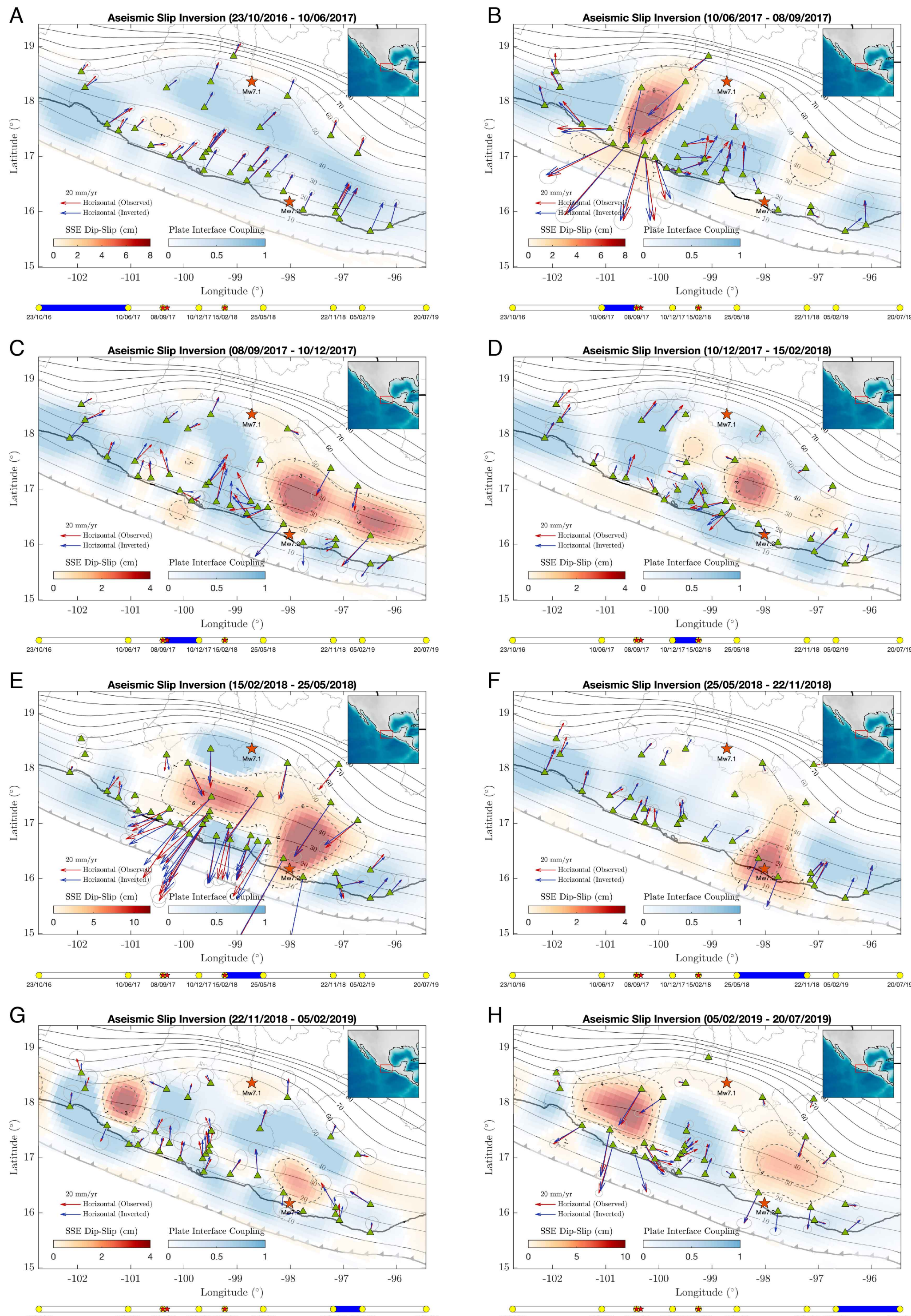


**Fig. 2.** Aseismic slip inversion results for the whole analyzed period across and after the earthquake sequence. Dashed slip contours are in centimeters. Yellow circles encompassing the

blue bar at the bottom of each panel indicate the dates of the associated inverted window, and red small stars, the Mw8.2 Tehuantepec, Mw7.1 Puebla-Morelos and Mw7.2 Pinotepa earthquakes timing, respectively, from left to right. Red and blue arrows show the observed and synthetic surface displacements, and the gray ellipses one standard deviation of the GPS data.

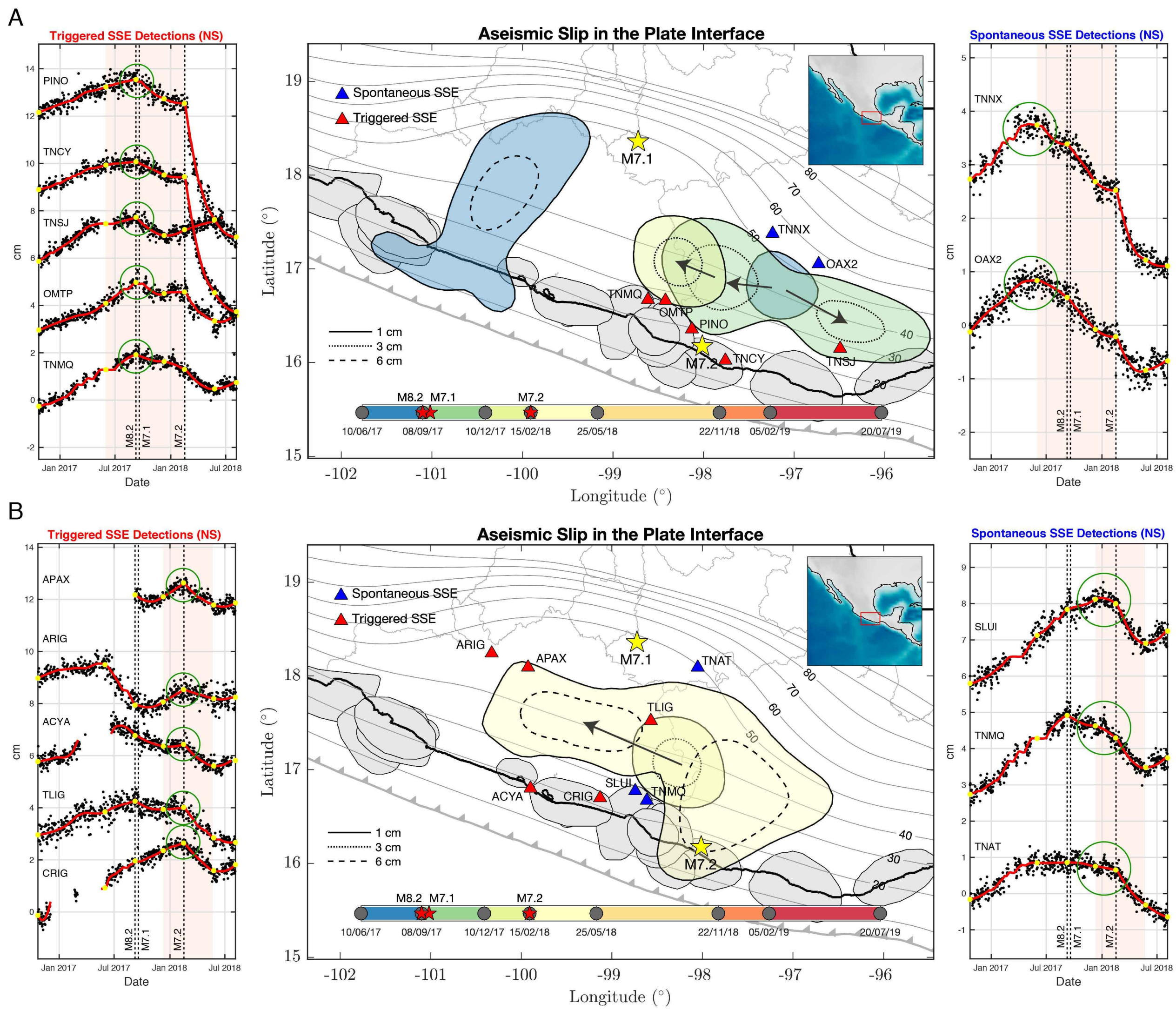


Fig. 3. Evolution of the aseismic (SSEs and post-slip) during the earthquake sequence. Pink shaded rectangles encompass the associated inverted windows for each panel (yellow dots). Blue triangles show GPS stations where spontaneously initiated or preexistent SSE are observed (right panels, green circles), while red triangles show the stations where triggered SSE are detected (left panels, green circles). Notice the abrupt reversal of the deformation pattern (from north to south) right when the Tehuantepec and Pinotepa earthquakes happened in the left panels (green circles).

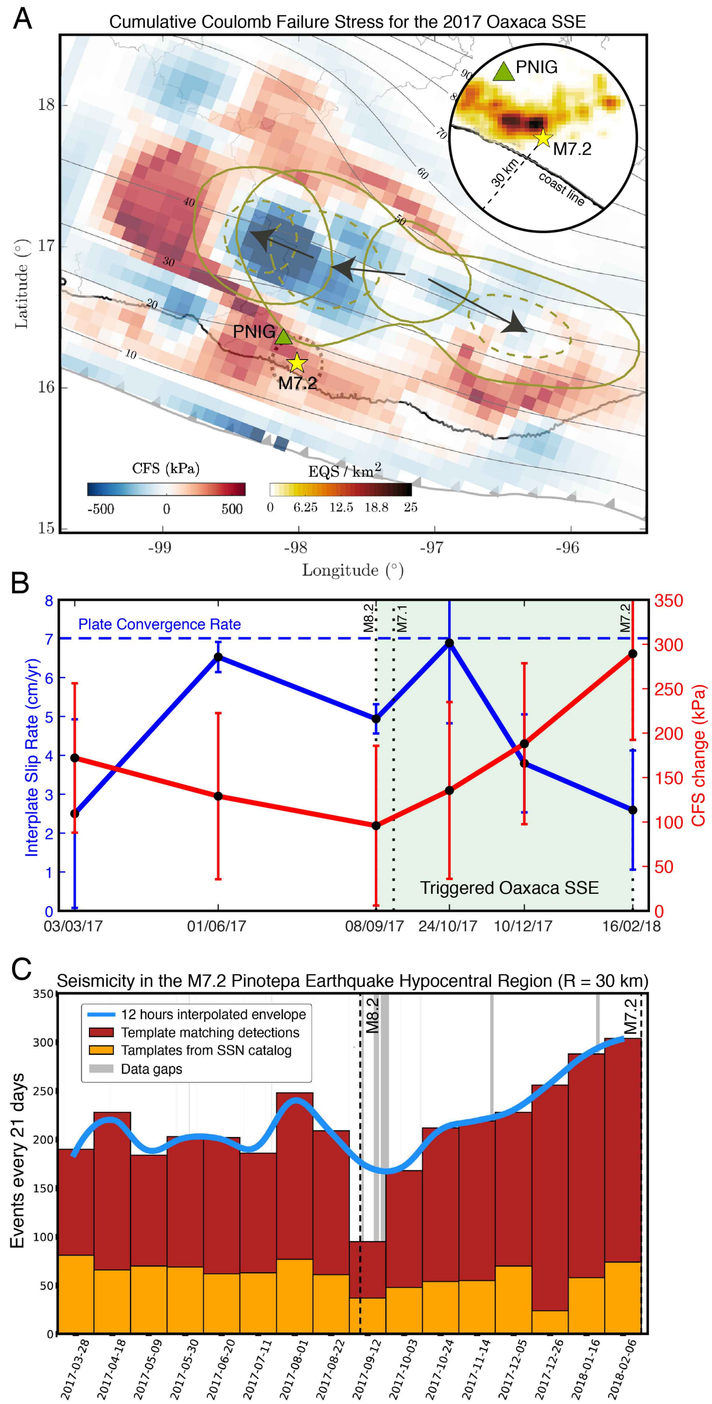


**Fig. 4.** CFS, PIC and seismicity rate evolution before the Pinotepa earthquakes nearby its hypocenter. (A) 15-month cumulative CFS on the plate interface and spatial evolution of the 2017 Oaxaca SSE (1 cm slip solid contours and 3 cm slip dashed contours). Density of TM precursor

detections (inset). (B) Temporal evolution of the CFS change and the interplate slip rate within a 20 km radius from the Pinotepa earthquake hypocenter (dotted circle, panel A). See also Fig. S4. (C) Seismicity rate evolution for M > 2.1 events within 30 km from the Pinotepa earthquake hypocenter.

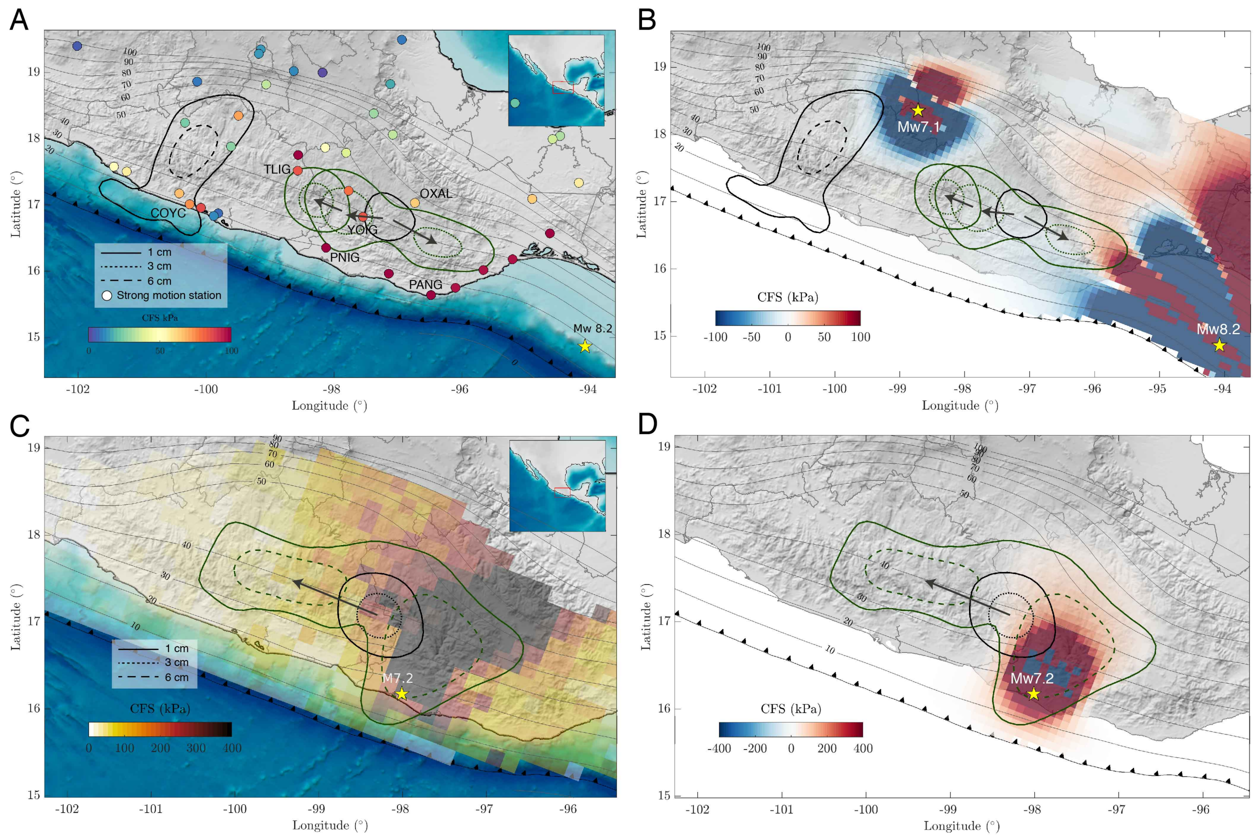


**Fig. 5.** Dynamic (peak values) and static CFSs on the 3D plate interface (gray contours) produced by the Tehuantepec (A and B, respectively) and Pinotepa (C and D, respectively) earthquakes in the plate convergence direction. Aseismic slip events right before the corresponding earthquake are shown with black contours, while those occurred immediately after the earthquake are shown with green contours. Dynamic stresses for the Tehuantepec event (A) where computed from actual strong motion records at different sites (colored circles, see Fig. S8A). Estimates for the Pinotepa event (C) where computed through a 3D finite-source numerical simulation of the earthquake (see Fig. S9).

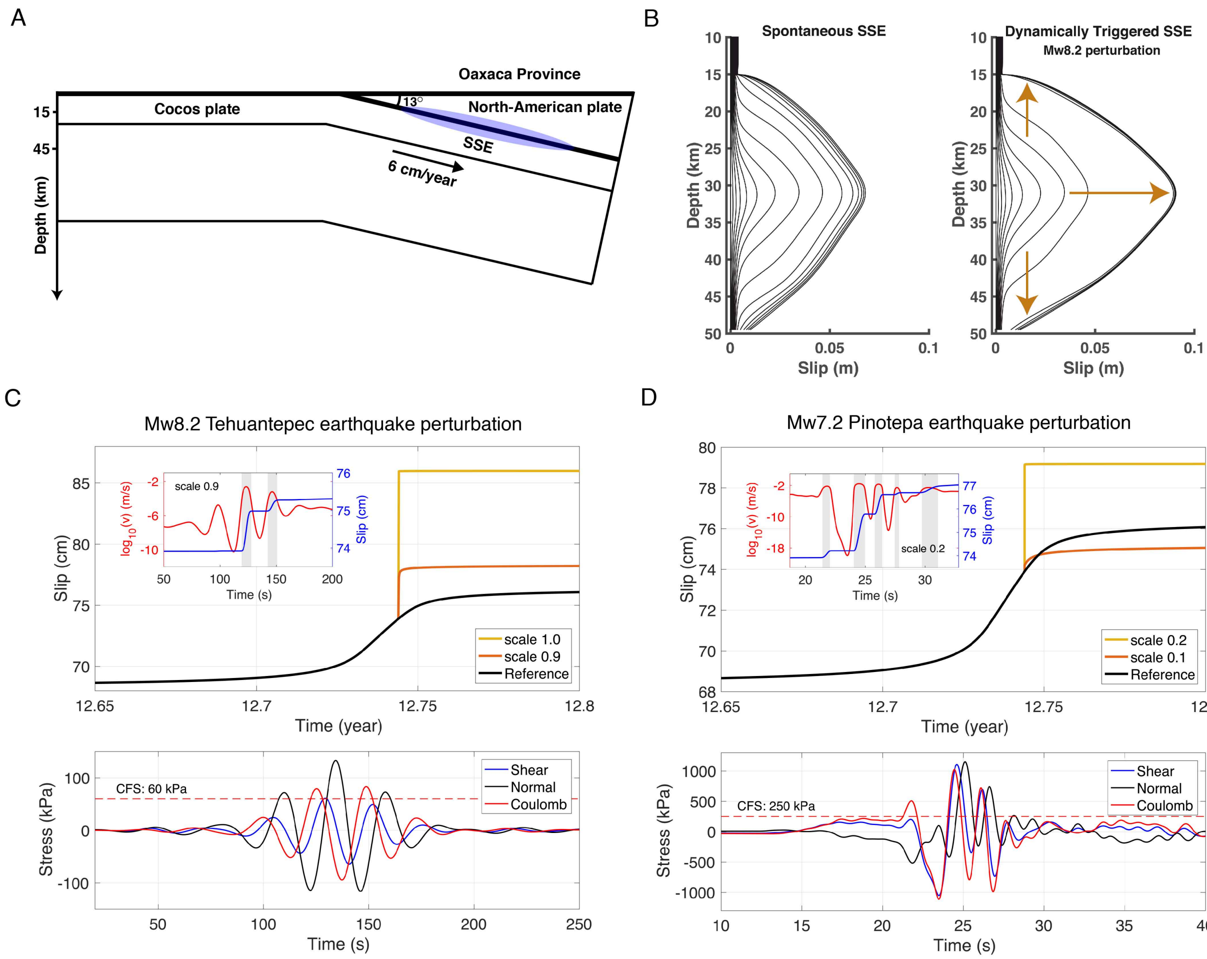


**Fig. 6.** Rate-and-state fault model for SSE triggering by seismic-wave stress perturbations. (A) Synoptic 2-D model of the subduction zone in the study area. (B) Slip evolution of a spontaneous SSE and a dynamically triggered SSE in the rate-and-state friction model. The contours time increment is about 2 days. (C) Top, slip evolution of the SSE reference model and two triggered events at 31 km depth for stress perturbations due to the Mw8.2 Tehuantepec earthquake with different scaling factors. The inset shows the slip velocity and slip at that depth with 0.9 scaled perturbation. Bottom, stress perturbation used in these simulations. (D) Same as (C) but for the Mw7.2 Pinotepa earthquake. Please note that the scaling factors are different.

| **Guerrero** | | | **Oaxaca** | | |
|---|---|---|---|---|---|
| **Aseismic Event** | **Date** (dd/mm/yy) | **Magnitude** (Mw) | **Aseismic Event** | **Date** (dd/mm/yy) | **Magnitude** (Mw) |
| SSE | 10/06/17 – 08/10/17 | 6.91 | SSE | 01/06/17 – 15/02/18 | 6.93 |
| SSE | 16/02/18 – 01/06/18 | 6.93 | Pinotepa Post-slip | 16/02/18 – 22/11/18 | 7.17 |
| SSE | 22/11/18 – 20/07/19 | 6.99 | SSE | 05/02/19 – 20/07/19 | 6.92 |

**Table 1.** Dates and moment magnitude (Mw) of all aseismic events reported in this work.

Supplementary Materials for

# Short-Term Interaction between Silent and Devastating Earthquakes in Mexico

**Authors:** V. M. Cruz-Atienza*, J. Tago, C. Villafuerte, M. Wei,

R. Garza-Girón, L. A. Dominguez, V. Kostoglodov, T. Nishimura,

S. I. Franco, J. Real, M. A. Santoyo, Y. Ito and E. Kazachkina.

*Correspondence to: cruz@geofisica.unam.mx

**This PDF file includes:**

## Methods

- <u>Elastostatic adjoint inversion</u>

The method used to invert the GPS time series, ELADIN (ELastostatic ADjoint INversion) (*25*), simultaneously determines the distribution of coupling and SSEs in the plate interface to explain the surface displacements. To this purpose, the method solves a constrained optimization problem based on the adjoint elastostatic equations with Tikhonov regularization terms, a von Karman autocorrelation function and a Gradient Projection method to guarantee physically-consistent slip restrictions. The main parameters governing the inversions are the correlation length of the von Karman function, $L$, which controls the wavenumber content of the solution, and the precision matrix, which weights the data according to its confidence. We assumed a von Karman Hurst exponent of 0.75 and $L$ = 40 km. Comprehensive resolution tests show that, given the problem geometry (i.e. the 3D plate interface and the available stations, Fig. 1), these values maximize the restitution index for slip patches larger than ~80 km length and minimize the data misfit error (*25*).

Although GPS data has been carefully processed to generate the displacement time series (see next section), there always remain trailing errors and physical signals that do not correspond to tectonic processes (Fig. S1). The precision matrix allows to minimize the effect of such noise in the inversion results and corresponds to the inverse of the data variance per station and time window. To do this, especially in the vertical component, numerous synthetic and real data inversions lead us to adjust the precision matrix (i.e., the data weights) to ensure that polarities of the vertical-displacement are well explained by the inverted models, while maintaining the best horizontal-displacement fits (*25*). The data variance for each component and time window is computed from the differences between daily displacement values and a moving, locally weighted LOESS function (i.e. 2nd order polynomial regressions with a half-window time support).

For the inversions we removed the coseismic displacements produced by the three large earthquakes and improved the 3D plate interface geometry introduced by Radiguet et al. (5) based on the work of Ferrari et al. (*36*), which compiles relocated seismicity, receiver functions and tomography studies in southern Mexico. We refined the final geometry beneath Oaxaca based on recent magneto-telluric and receiver function analysis (*37, 38*) (Fig. 1) and assumed a suitable 1D four-layer regional structure (*39*). The slip vector is decomposed in the plate-convergence (pc) and pc-perpendicular directions, which vary along the plate interface (*40*). Restrictions were imposed to meet reasonable plate coupling constraints (i.e. backslip smaller than the cumulative plate motion in the associated time window) and moderate pc-perpendicular slip by means of an iterative Gradient Projection method (*25*), so that the slip rake could only vary 30 degrees with respect to the plate convergence direction.

- GPS data processing

We used continuous records in 57 permanent GPS stations spread across central Mexico (Fig. 1). The stations belong to three different networks: the Mexico-Japan SATREPS-UNAM project (*24*), the National Seismological Service (SSN-UNAM) and Tlalocnet (*41*). GPS data was processed using two different methods: Gipsy 6.4 (*42*) and Gamit/Globk 10.7 (*43*). For the period between October 23 (2016) to November 22 (2018), after carefully comparing both displacement timeseries in all stations, we selected those with better signal to noise ratio and consistency with nearby stations (Fig. S1A). For the period from November 22 (2018) to October 8 (2019), we only considered selected timeseries calculated using Gipsy 6.4 (Fig. S1B).

The GIPSY displacement timeseries are estimated with a Precise Point Positioning strategy. The station positions are defined in the International Terrestrial Reference Frame, year 2014 (ITRF

2014). For daily processing we used the Jet Propulsion Laboratory final and non-fiducial products (orbits and clocks). We generated observables using 2 model categories: (1) Earth models and (2) observation models. The Earth models include tidal effects (i.e. solid tides, ocean loading and tide created by polar motion), Earth rotation (UT1), polar motion, nutation and precession. Observation models, on the other hand, are related with phase center offsets, tropospheric effects and timing errors (i.e. relativistic effects). The troposphere delay is estimated like as random walk process. This effect is broken into wet and dry components. The azimuthal gradient and the dry component are estimated using GPT2 model and mapping function (TGIPSY1). The antennas phase center variations are considered through antenna calibration files. For receiver antennas, the correction is estimated taking the International GNSS Service (IGS) Antex file. We also applied a wide-lane phase bias to account for the ambiguity resolution and removed outliers.

The GAMIT displacement timeseries are estimated using a double difference method that calculates the between-station and satellites differences. It reduces satellite clock and orbit errors, localized atmospheric errors and cancels the effects of variations in the receiver clocks. The software incorporates final IGS (International GNSS Service) combination solutions for orbits (with accuracies of 1-2 cm) and Earth Orientation Parameters (EOP). Ionospheric and atmospheric corrections were applied during processing. Hydrostatic and water vapor delay are corrected using Vienna Mapping Functions (VMF). Solid Earth tide model (IERS03), ocean tidal loading (FES2004), tables for earth rotation values (nutation IAU2000, polar motion, universal time) and precession constant IAU76 are applied. The resulting GPS time series are calculated in the ITRF 2014 reference frame and then rotated with respect to the fixed North American plate using the rotation pole. Post-processing of daily position time series includes offset corrections and outlier removal that was performed with the help of python-based PYACS package developed by J.-M. Nocquet.

- <u>Template-matching seismicity analysis</u>

To detect unreported seismicity within the Mw7.2 Pinotepa earthquake hypocentral region previous to the event, we applied two independent and complementary template matching (TM) techniques. In both cases, the waveform templates were earthquakes reported by the SSN with foci within 30 km from the Pinotepa earthquake hypocenter (Lat: 16.218º, Lon: -98.014º, 16 km depth). We used continuous velocity records in three broadband stations with epicentral distance smaller than 115 km during a one-year period preceding the earthquake, from March 1, 2017, to February 16, 2018 23:39 (UTC time of the Mw7.2 earthquake).

The first technique (*44*) considers three permanent stations (PNIG, YOIG, TXIG) from the SSN network located in the state of Oaxaca (Fig. S5A). We used a set of 394 events (templates) reported in the SSN catalog and applied a bandpass Butterworth filter with corner frequencies of 1-8 Hz to reduce the noise, and to remove undesired regional and teleseismic events. For each template, we selected a cross-correlation window starting 1 seconds before the arrival of the S-wave and ending 5 seconds after, only one detection is allowed every 25 seconds to avoid duplicates of the same event. A detection was confirmed when the stacked correlation coefficient (scc) in the three stations (nine channels) was larger than 0.41 and the median average deviation larger than 25 (Fig. S5C). To this end we performed a grid search in a plane of 4.5 km x 4.5 km around each template location (Fig. S5A) and looked for the maximum scc value. For preventing detectability variations, we only processed those days with data for all components in the three stations.

The second technique considers only the waveforms on the three channels of the station PNIG, the closest site to the earthquake epicenter (21 km, Fig. S5B). For generating the templates, we selected 4,105 events from the catalog reported by the SSN in the period between March 1, 2017 and March 31, 2018. The waveforms where cut 0.2 seconds before the P-phase arrival and 0.5 seconds after the S-phase arrival, and filtered using a zero-phase Butterworth bandpass filter with corner frequencies at 3 Hz and 12 Hz. The template matching was performed using the Python package EQcorrscan (*45*) and the detection threshold was set to 0.9 of the average cross-correlation value in the three channels. Single-station detections have proved to be a powerful tool to find earthquakes that are small and located close to certain stations, but that get too attenuated to be detected at farther stations given high cross-correlation thresholds (*46*). Furthermore, a visual inspection of hundreds of waveforms helped us verify that the timing and the relative amplitudes of the ballistic P and S waves in the three components are very similar to the parent templates, guaranteeing that the detected signals are, indeed, earthquakes that share a common hypocentral location as the template events (Fig. S5D). For this second matched filter technique we allow inter-event times to be greater or equal to 10 seconds, keeping only the best correlated detections.

To assign a common magnitude to all detections, $M_L$, we determined an attenuation relationship specific to PNIG using the LocMagInv code *(46)* (Fig. S6A). Instead of inverting for the magnitudes, we used the cataloged magnitudes from the SSN for events with SNR greater or equal to 5 and inverted only for the geometric spread, attenuation and station correction parameters from horizontal displacement records (mm) (i.e. arithmetic mean). To obtain the displacements, we integrated velocity records in the bandwidth 3-12 Hz. We only used the available horizontal components for each event.

We detected 3,156 events with the first technique (Fig. S5A) and 5,064 with the second (Fig. S5B), which represent a 180% and 350% detection increase, respectively, as compared with the 1,125 earthquakes reported by the SSN in the same period and within a 30 km hypocentral radius. Detections from both techniques were integrated into a single catalog avoiding duplicate events (Fig. 4D). Figure S6C shows the frequency-magnitude histograms for both, our TM detections and the SSN catalog, where the cutoff completeness $M_L$ magnitudes correspond to 2.1, 2.4 and 3.2, for local detections (method two), regional detections (method one) and the SSE catalog, respectively. Since TM method one uses nine seismic channels (i.e. the three components of three stations) at a regional scale, its detections very likely correspond to events with hypocentral locations close to those of the templates that lie, all of them, within 30 km from the Pinotepa earthquake hypocenter. Thus, we used these detections for relatively large events to check how well method two, which only considers local records at PNIG (i.e. the three component), detected earthquakes within such hypocentral vicinity. Figure S6D show a Venn diagram for all catalogs where we see that 72% of regional detections were also found using only local records.

- Dynamic Perturbations at the Plate Interface

From Strong Motion Records: For the Mw8.2 Tehuantepec event we used radial and vertical displacement records at 25 s period from strong motion stations in south-central Mexico (Figs. 5A and S7C) to estimate the strain field produced by the Rayleigh waves fundamental mode at depth, and then the associated CFS (apparent friction coefficient of 0.5) over the 3D plate interface in the plate-convergence slip direction (Fig. S8A). Values in Fig. 5A at sites without interface below correspond to a horizontal surface at 50 km depth.

To estimate the surface-wave dynamic deformations (and tractions) at depth from observed ground displacements (i.e. double integration of single-station strong motion records) we followed a two-fold procedure: First, we estimated the displacement at depth (i.e. at the plate interface below each site, Fig. 5A) by modulating the field with the associated surface waves eigenfunctions for the chosen period within a four-layer regional model determined from the dispersion of surface waves (*39*) (Fig. S7D). Then, to estimate the whole stain tensor, we computed the horizontal deformations assuming a phase velocity of 3.5 km/s (*31*), and the vertical deformations by deriving the eigenfunctions in that direction. Although Love waves can also have SSE triggering potential, in the analysis we only considered perturbations from Rayleigh waves. Figure S8 shows, for the Mw8.2 Tehuantepec earthquake, the traction vector and CFS time series on the 3D plate interface along the plate-convergence slip-rate direction and dilation time series below some selected sites.

To validate our procedure, we compared estimated (with our method) synthetic tractions with the exact solution for the Lamb's problem (i.e. for the wavefield excited by a single vertical force on top of a homogenous halfspace) at depth over a horizontal plane (Figs. S7A and S7B). The elastic properties of the medium are $\alpha = 5.6$ km/s, $\beta = 3.233$ km/s, $\rho = 2700$ kg/m$^3$, the surface station lies 300 km away from the source and the buried point is 20 km below the station. In this example, tractions were estimated for 10 s period. However similar, satisfactory results were obtained for different periods and depths.

<u>From 3D Numerical Simulations:</u> To estimate the Mw7.2 Pinotepa earthquake (complete-wavefield) dynamic perturbations at the plate interface we performed a 3D kinematic-source numerical simulation by means of an hp-adaptive discontinuous Galerkin finite-element method (DGCrack) (*33*). The domain is discretized with a non-structured tetrahedral mesh considering a 3D crustal velocity model of the Guerrero-Oaxaca subduction zone (*47*) that incorporates the real topography

and bathymetry, as well as the geometry of the plate interface (Fig. S9A). The mesh size is 900 x 380 x 104 km in the along-trench, trench-perpendicular and vertical directions, respectively, with approximately 11 million elements to achieve a numerical accuracy up to 1 Hz. We run DGCrack in 512 cores on the UNAM supercomputer platform Miztli to complete 260 seconds of numerical simulation spending 12.5 hours of total computer elapsed time. To simulate the finite source, we first used the low-wavenumber slip solution of the Pinotepa earthquake estimated by the USGS (Fig. S9B-up). Then, we discretized this solution into subfaults of 1 x 1 km and add high-wavenumber slip perturbations that are stochastically generated using a von Karman power spectral density (PSD) function to enhance the radiation of high frequencies following the methodology of Pulido et al. (*48*) (Fig. S9B-down). The slip-rate of every subfault follows a regularized Yoffe function and the rupture evolution is described by the spatial distribution of the slip, rise time, rupture velocity and peak time (i.e., the time to reach the peak slip-rate in every subfault) (Fig. S9C). These kinematic source parameters are heterogeneously distributed by means of a pseudo-dynamic rupture generator that considers the 1-point and 2-point statistics of each source parameter as well as their spatial interdependency extracted from dynamic rupture simulations. We validate the earthquake simulation by comparing the horizontal geometric mean of the observed and synthetic peak ground velocities (PGV) in different hard-site strong motion stations (Fig. S9D).

Since the resolution of the GPS time series does not allow distinguishing whether the Tehuantepec or Puebla-Morelos earthquakes (only eleven days in between them) produced the abrupt change of the crustal deformation pattern observed in Fig. 3A, we also estimated the dynamic perturbations on the plate interface due to the intraslab, normal-faulting, Mw7.1 Puebla-Morelos event using the same numerical procedure but taking a finite-source solution determined from the inversion of strong motions (*17*). Results are shown in Fig. S3F, where we appreciate that CFS peak values in the 2017 Oaxaca SSE region (apparent friction coefficient of 0.5) are smaller than those induced by the Tehuantepec earthquake (Fig. 5A) (i.e. < 60 kPa). Considering also that the duration of intense shaking by the Mw7.1 is much shorter than that produced by the Mw8.2 Tehuantepec event (i.e. its SSE triggering potential is lower, Fig. S10D) and that tremor activity in Oaxaca highly increased a few hours after the Tehuantepec earthquake (*23*), then we conclude that triggering of the 2017 Oaxaca SSE was produced by seismic waves from the Mw8.2 event.

- Rate and State Friction SSE Model

Assuming a 6 cm/yr plate convergence (*40*), we developed a R&S fault reference model for the Oaxaca region that spontaneously generates SSEs every 1.5 years with maximum slip of ~10 cm (Fig. S10C), which is a reasonable approximation of the SSE activity in that province (*21*). The model assumes a planar fault dipping 13 degrees in a 2D elastic half-space (Figs. 6A and S10A). Following Wei et al. (*34*) and based on the SSEs slip distributions (Figs. 2C and 3A), the model is consisted of a velocity-weakening (VW) fault segment between 20 and 45 km depth where SSEs take place encompassed by stable, velocity-strengthening (VS) layers (Fig. S10B). Uniform, dynamic stress perturbations from the 2017 Mw8.2 Tehuantepec earthquake and the 2018 Mw7.2 Pinotepa earthquake were inputted around the middle stage of a spontaneously initiated SSE at all depth with different scaling factors (Fig. 6) to consider the variations and uncertainties of both, the reference model and the CFS estimates throughout the SSE region.

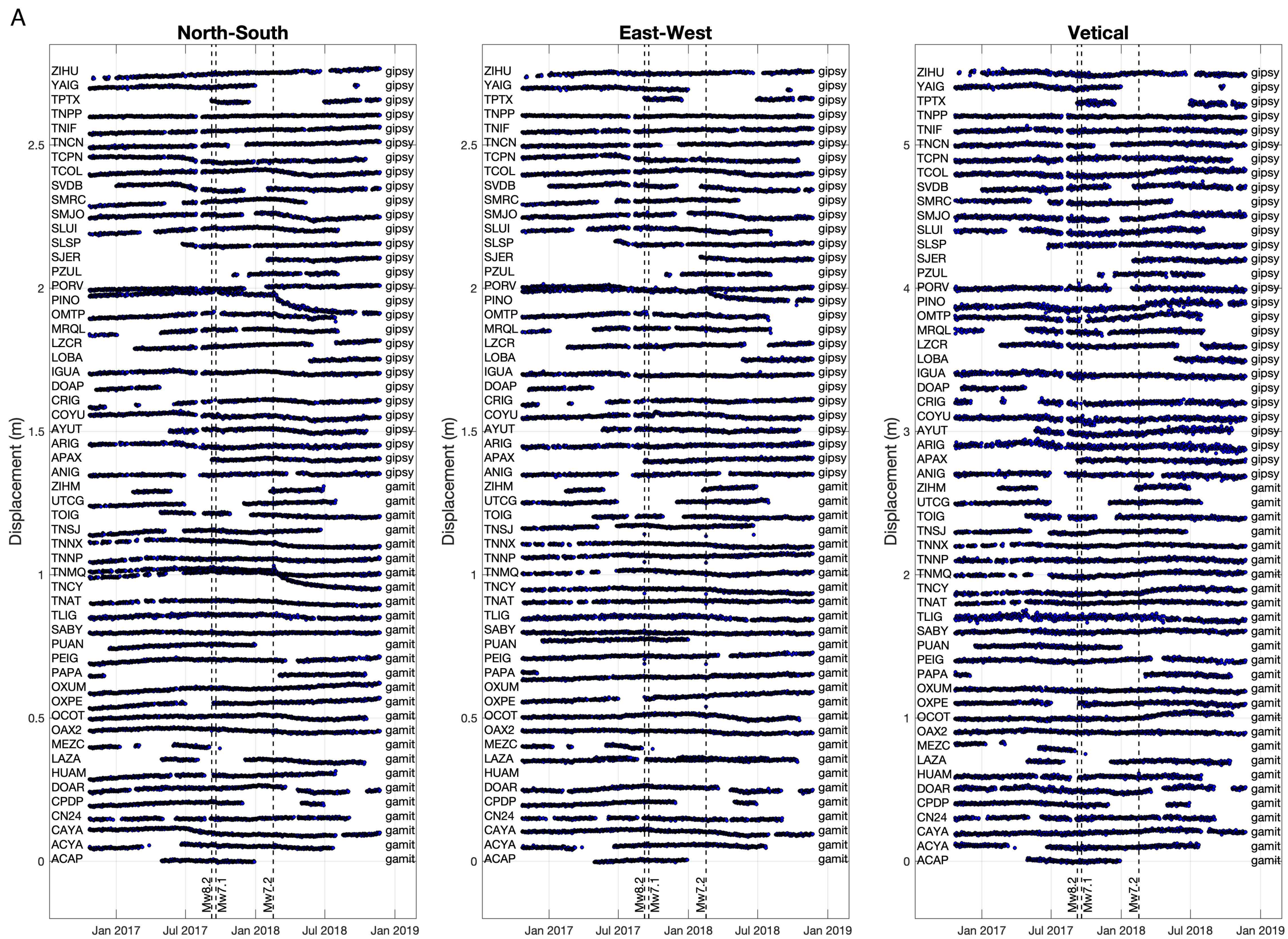


**Fig. S1.** Displacement GPS time series in 57 selected stations (A) from October 23 (2016) to November 22 (2018) and (B) from November 22 (2018) to October 8 (2019). To the right of each series is indicated the data processing method selected for the inversions. Vertical dashed lines indicate the occurrence of the three earthquakes of the sequence.

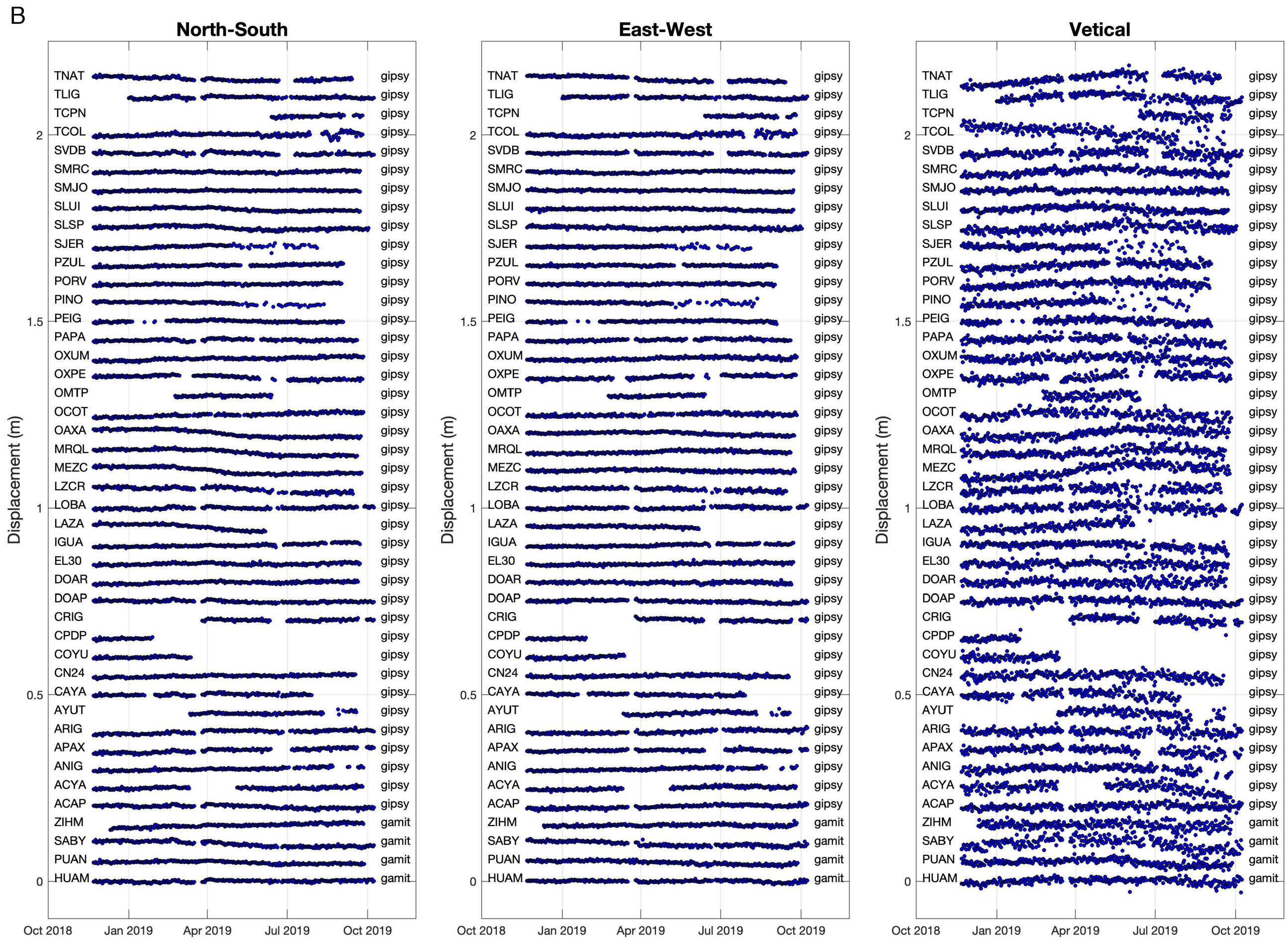


**Fig. S1** (Continuation).

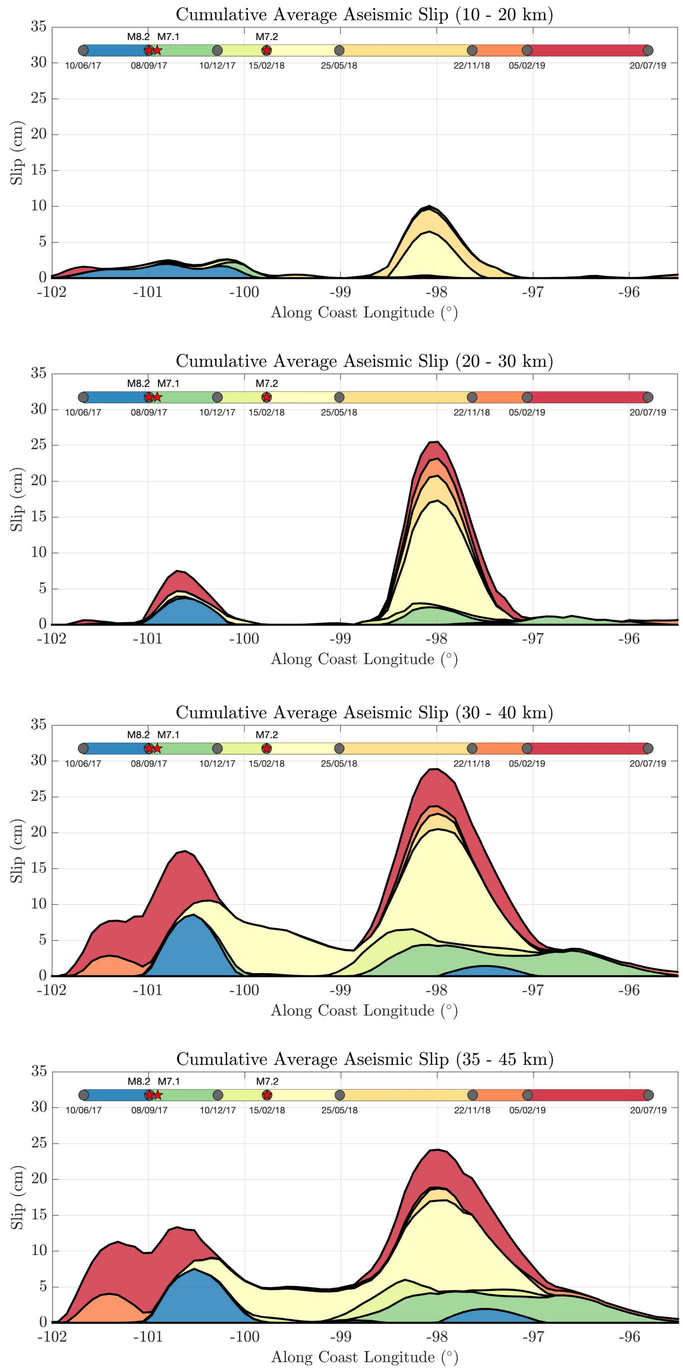


**Fig. S2.** Cumulative slow slip time history, averaged for different depth ranges (see panel titles), from solutions shown in Fig. 2. Between 10 and 20 km depth (i.e. mainly offshore), only the 2017 Guerrero SSE and the Pinotepa earthquake post-seismic slip are significant, with maximum slip of 2.0 and 6.5 cm, respectively. The largest SSE activity concentrates between 20 and 45 km depth.

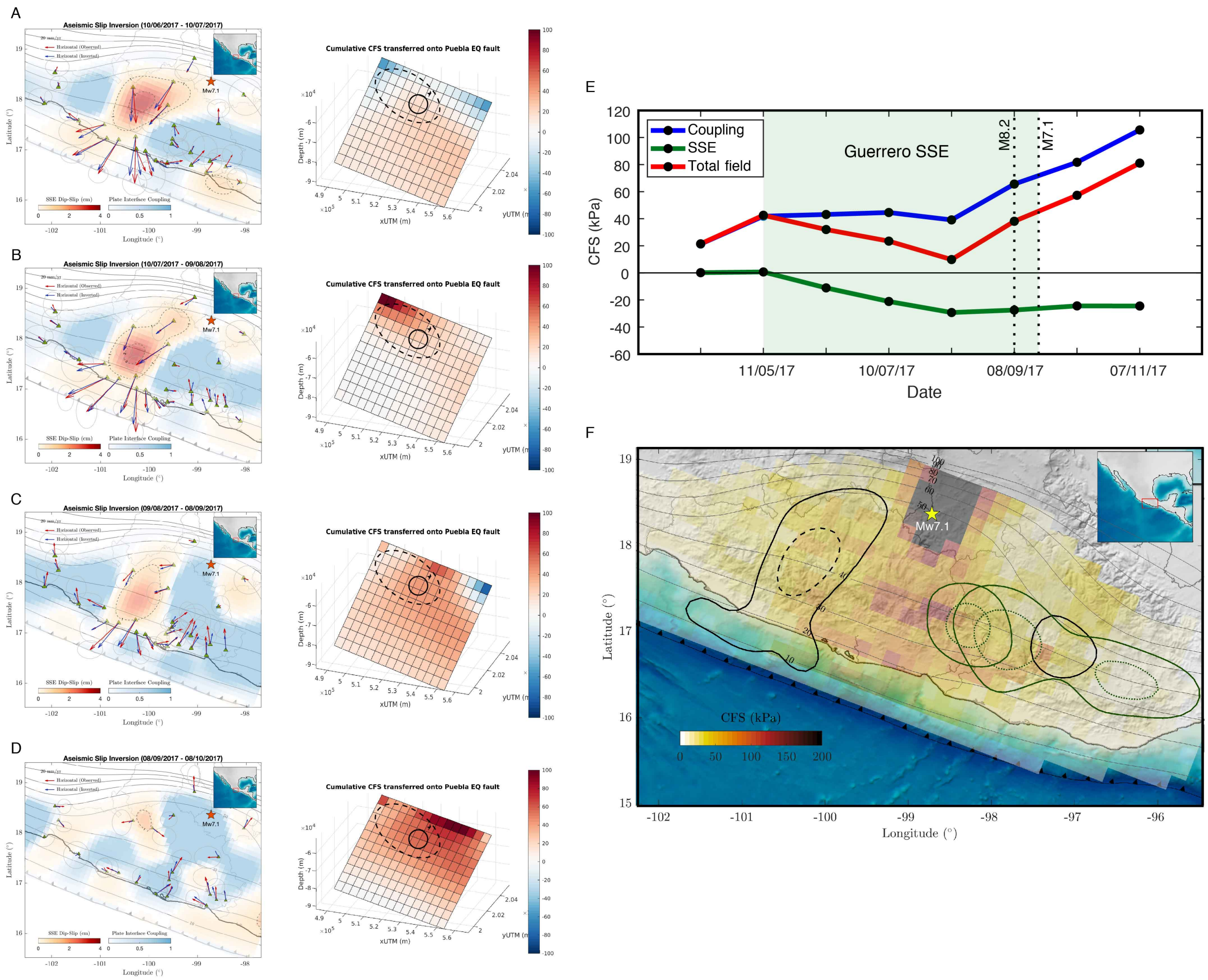


**Fig. S3.** (A-D) 30-day time windows aseismic slip inversions of the 2017 Guerrero SSE (left column) and the associated cumulative CFS over the intermediate-depth normal fault where the Mw7.1 Puebla-Morelos earthquake took place on September 19, 2017 (right column). Notice that the inverted time windows are shorter than those shown in Figs. 2 and S2. (E) CFS evolution within a 20 km radius from the Puebla-Morelos hypocenter. Notice the CFS sustained increment induced by the PIC in the later SSE stage. (F) CFS maximum values on the plate interface induced by the Puebla-Morelos earthquake. They were estimated with a 3D finite source simulation (see Fig. S9) similar to that performed for the Pinotepa earthquake (Fig. 5C) but using the finite-source solution determined by Mirwald et al. (*17*). Aseismic slip events right before the earthquake are shown with black contours, while those occurred immediately after the earthquake are shown with green contours.

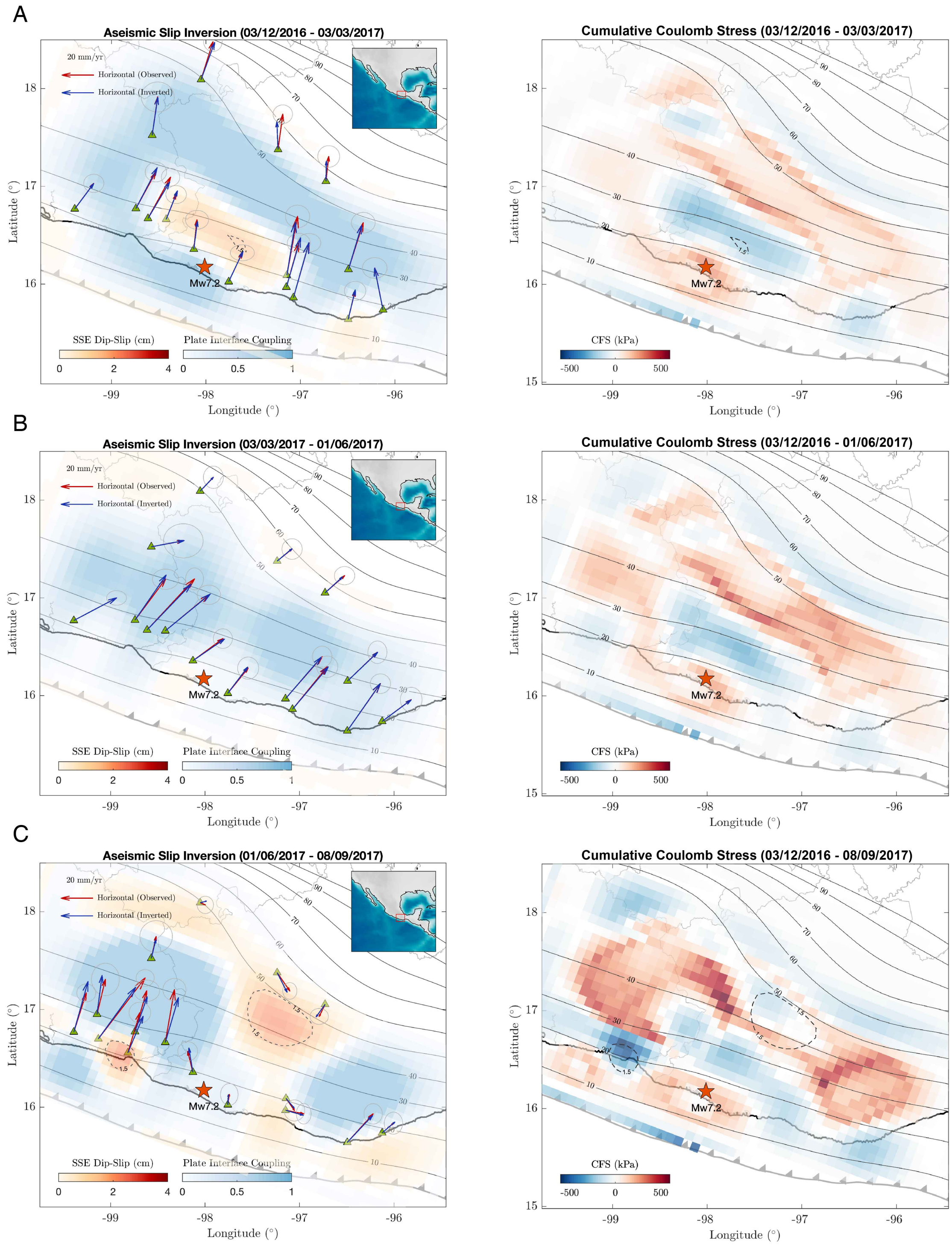


**Fig. S4.** Aseismic slip inversions preceding the Mw7.2 Pinotepa earthquake during the 2017 Oaxaca SSE (left column) and the associated cumulative CFS on the plate interface (right column). Dashed contours in the right column show the aseismic slip contours of the associated time window. Notice that the inverted time windows are shorter than those shown in Fig. 2. Average CFSs from these higher time-resolution inversions are shown in Fig. 4B.

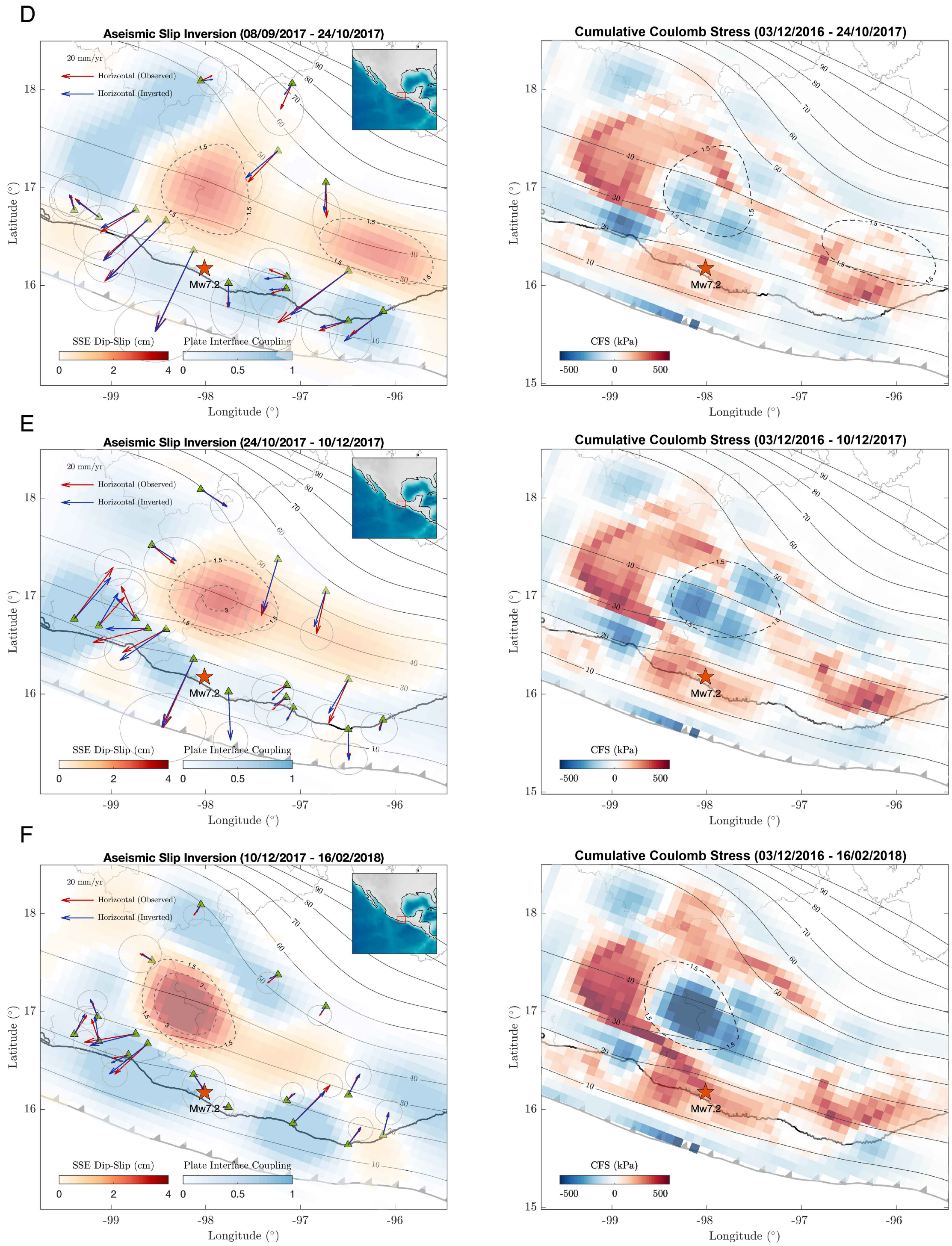


**Fig. S4.** (Continuation).

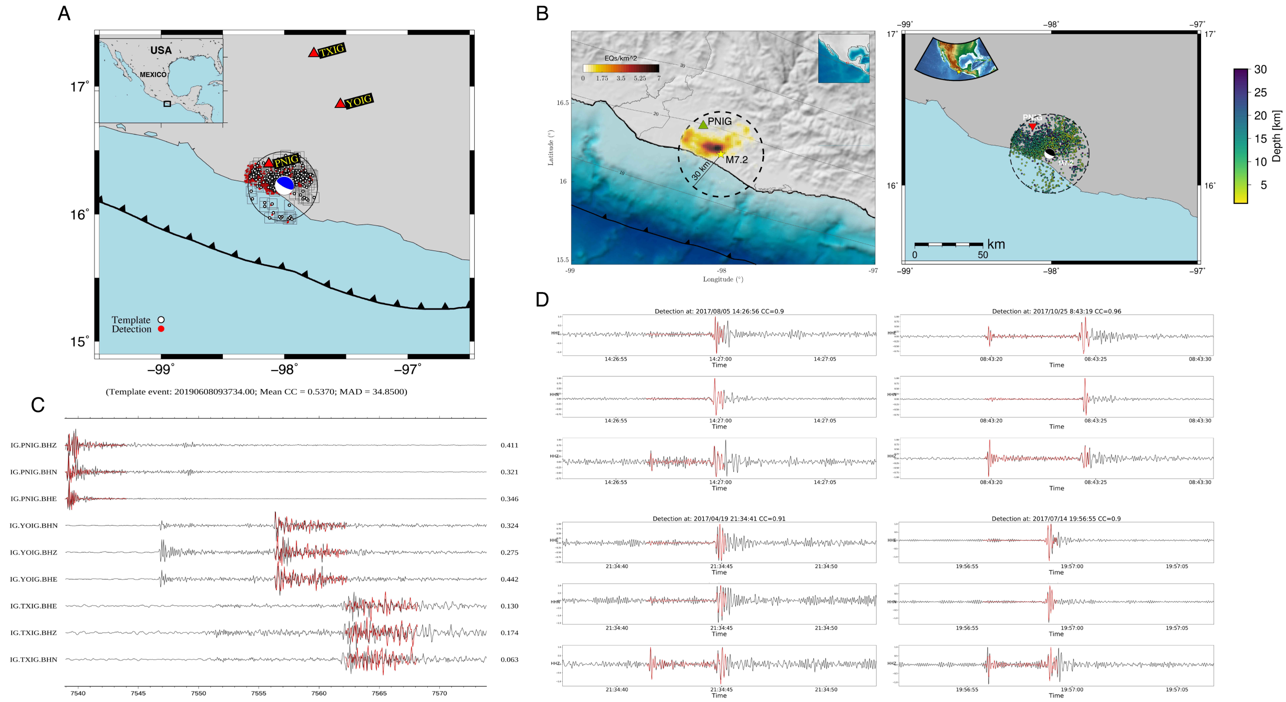


**Fig. S5.** Illustration of template matching results using two different methods. (A) Map of events detected by method 1 using three stations at a regional scale. (B) Density map for the template events used by method 2 (left) and their spatial distribution (right). (C) Example of a regional detection made at stations PNIG, YOIG and TXIG using method 1 for the direct S wave and its coda. (D) Examples of local detections made at station PNIG using method 2. The good fits of the templates that include both P and S direct waves and the coda of the P waves guarantee that detections come from the same hypocentral locations as the template events. See Figure 4 of the main text.

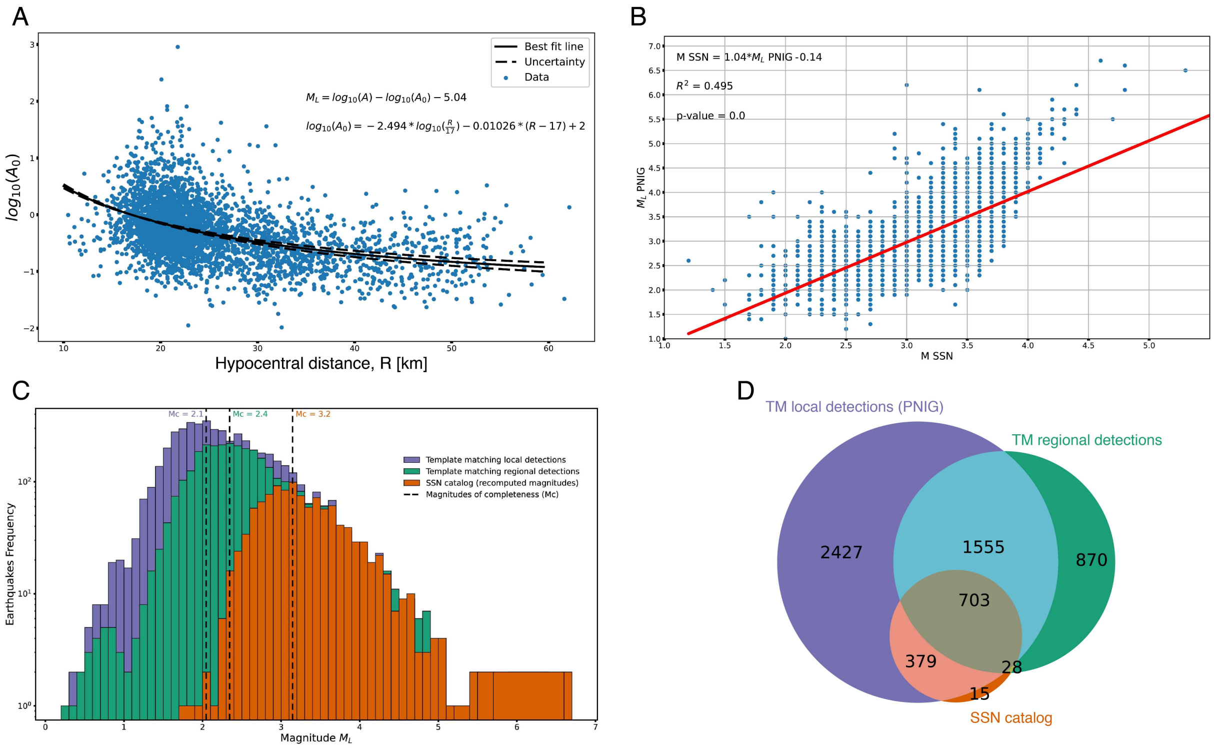


**Fig. S6.** Magnitude estimation for the template-matching (TM) newly detected earthquakes and final catalogs comparison. (A) Attenuation relationship calculated on the horizontal components (geometric mean) of PNIG and magnitude scale $M_L$. (B) Correlation between recomputed $M_L$ magnitudes using the PNIG station and the magnitudes reported by the SSN. (C) Earthquake frequency distributions for the template matched catalogs using the closest station PNIG (blue), three stations of the regional network (green) and the catalog provided by the SSN (orange). (D) Venn diagram showing the relationship of the number of events of each catalog. The intersections are calculated by finding common events in time (events within 10 seconds of each other).

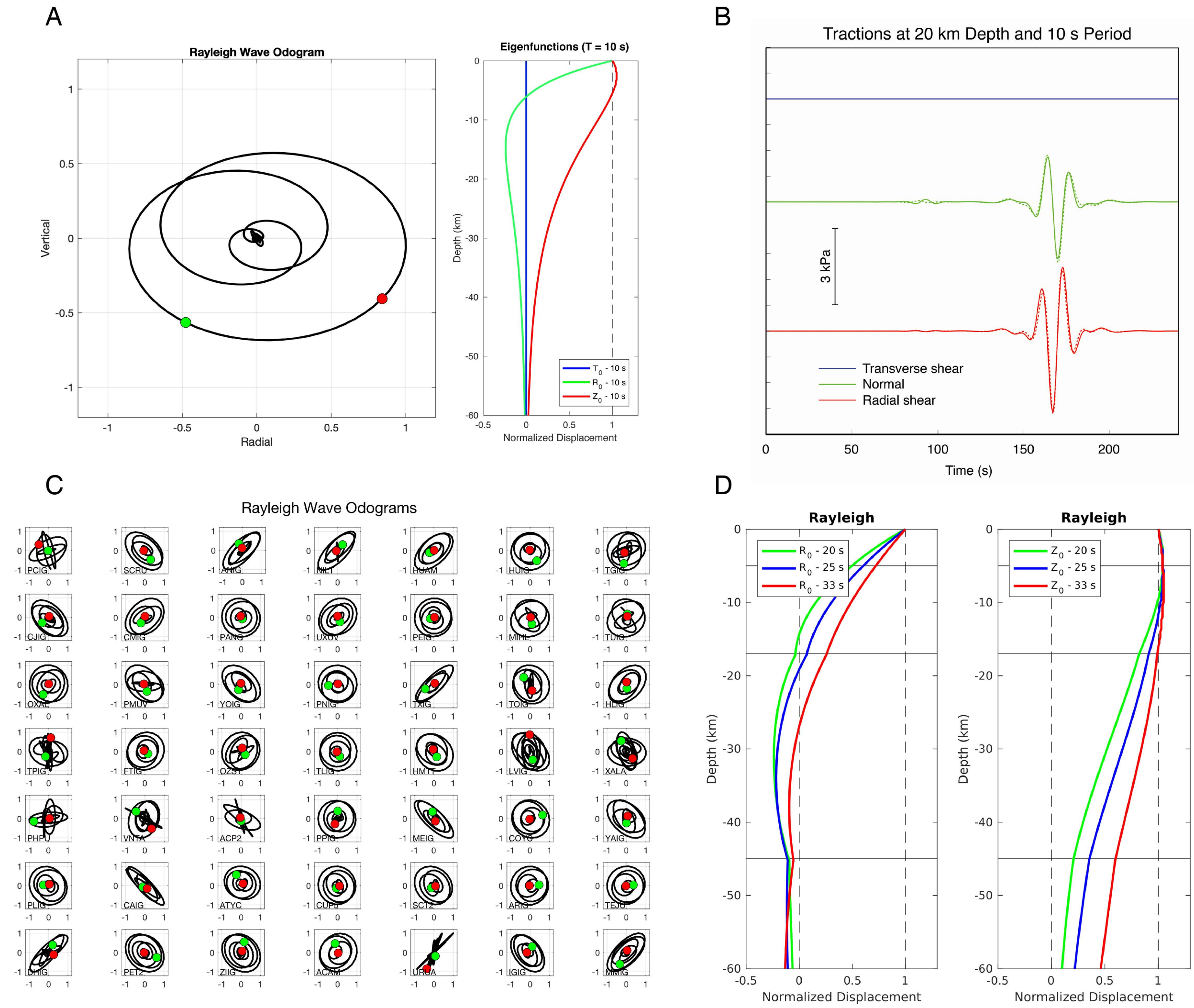


**Fig. S7.** Validation of the procedure to estimate dynamic perturbations on the plate interface from actual strong motion records. (A) Odogram of a Lamb pulse (i.e. of the wavefield produced by a vertical force applied at the free surface of a homogeneous halfspace) (left), and corresponding eigenfunctions for the Rayleigh wave fundamental mode at 10 s period (right). (B) Comparison at 20 km depth (horizontal plane) and 10 s period of the exact traction evolution (solid) and the estimated traction following the procedure described in Methods (dashed). (C) Odograms for the radial and vertical displacement components around 25 s period from actual records of the Mw8.2 Tehuantepec earthquake on 49 strong motion station (see Fig. S8). (D) Eigenfunctions of the

Rayleigh waves fundamental mode in a crustal 1D velocity model (*39*) used to estimate beneath each station the traction, CFS and dilation evolution on the 3D plate interface shown in Figs. 5A and S8.

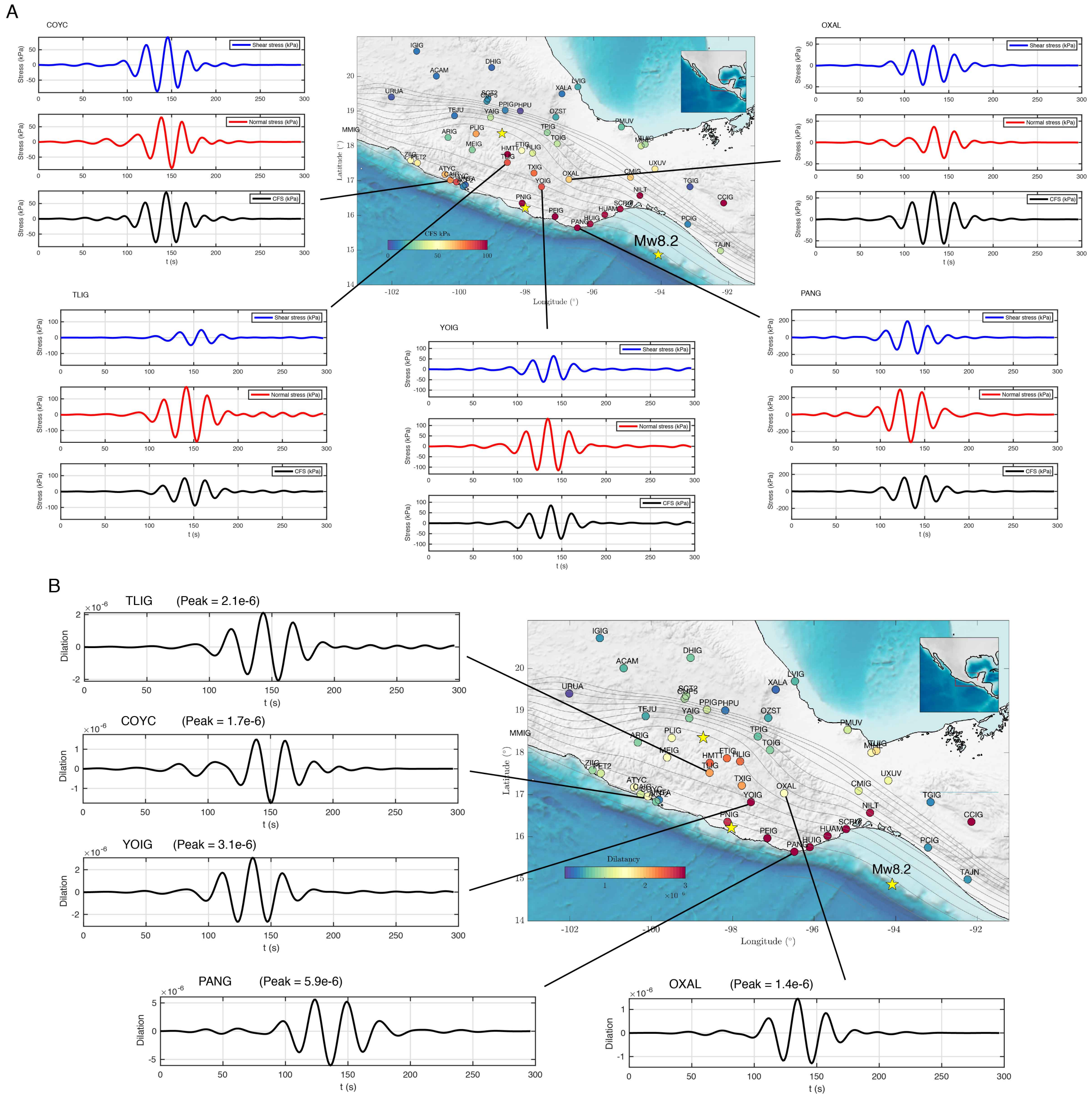


**Fig. S8.** 20 s period dynamic-stress (A) and dilation (B) perturbations over the 3D plate interface (gray contours) estimated from actual strong motion records of the Mw8.2 Tehuantepec earthquake below different seismic stations (circles). CFSs (computed in the plate-convergence slip direction) and dilations peak values are color-coded in each site. Values where there is no plate interface below correspond to 50 km depth over a horizontal surface.

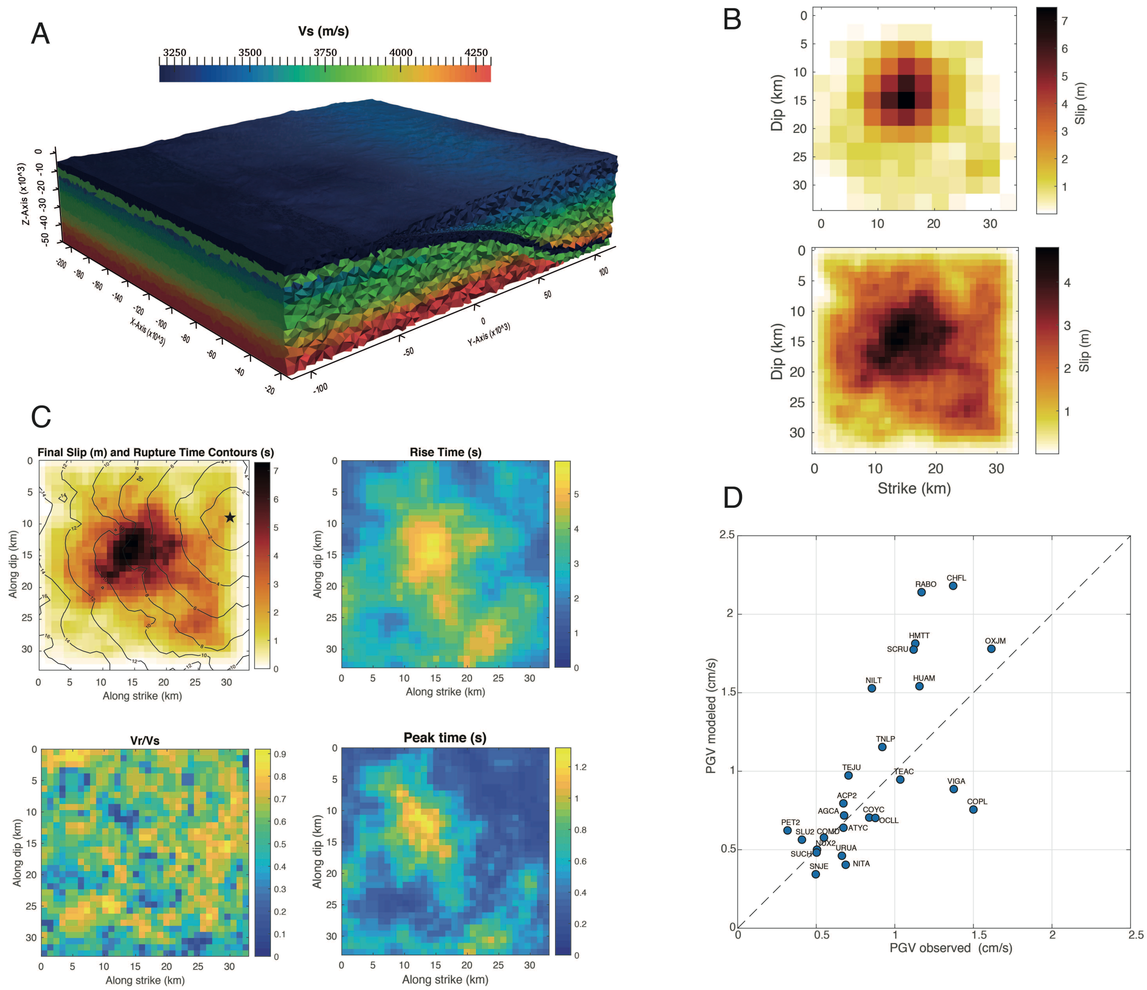


**Fig. S9.** 3D kinematic finite-source numerical simulation of the Mw7.2 Pinotepa earthquake. (A) Non-structured tetrahedral discretization of the Oaxaca subduction zone. (B) Initial USGS finite source inversion (up) and broad-band wavelength finite slip model (bottom). (C) Spatial distribution of the slip, the rise time, the rupture velocity and the peak time used to describe the kinematic rupture evolution. (D) Comparison between modeled and observed horizontal PGV for different hard-site strong motion stations (see Fig. S8 for site locations).

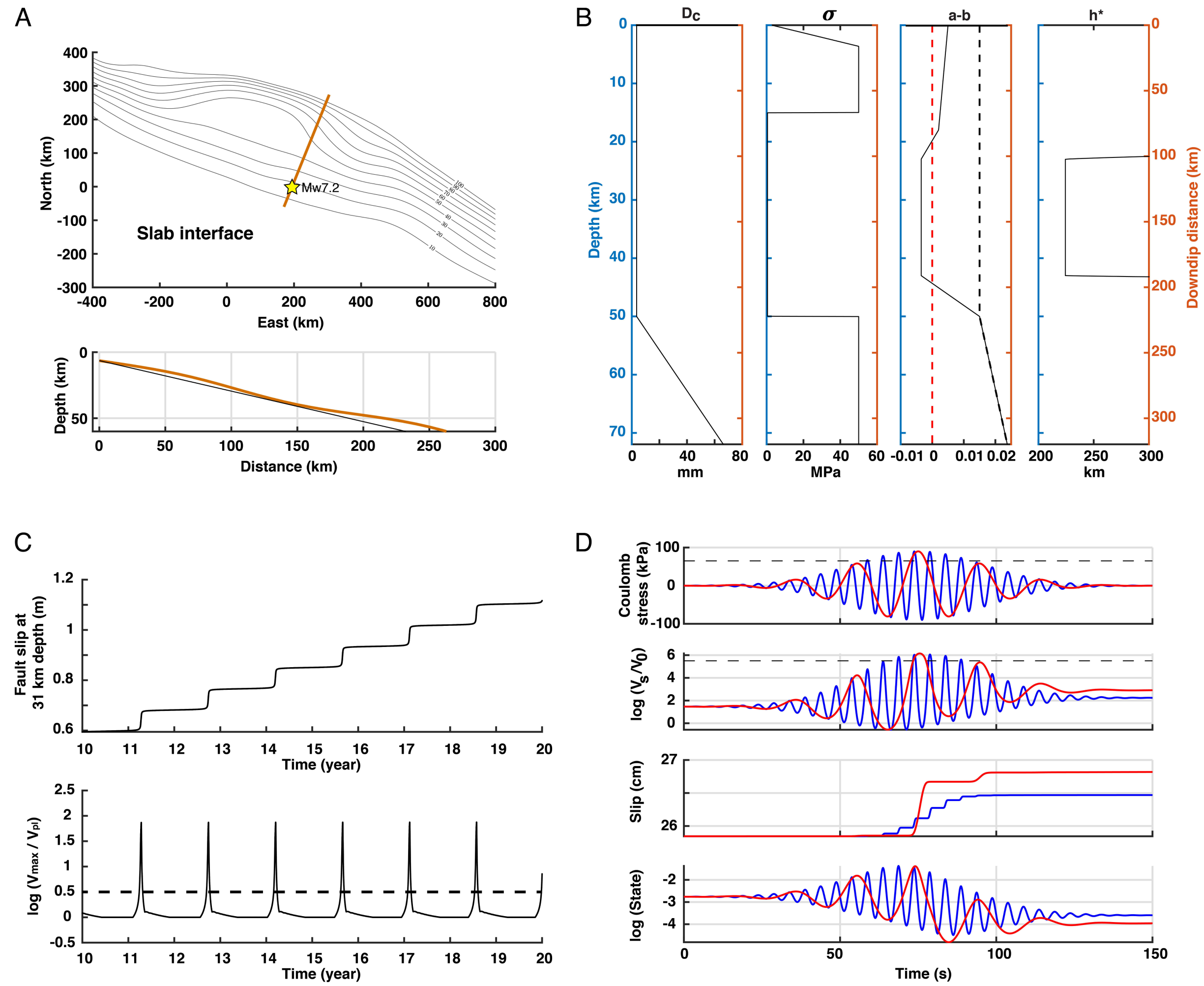


**Fig. S10.** (A) Top, slab geometry in the study area across the 2018 Mw7.2 Pinotepa earthquake epicenter. The orange solid line shows the profile of our 2D model over the 3D plate interface geometry. Bottom, the black solid line shows the planar fault model and the orange line shows the slab geometry. (B) Rate-and-state parameters used in our 2D reference model. Dc above 50 km is 3.5 mm. The effective normal stress in the low stress zone is 0.45 MPa. (C) Slip at 31 km depth and the maximum slip rate on the fault for the reference model. (D) Evolution of key model parameters with two different perturbations with different characteristic periods (5 s and 20 s periods) and same 60 kPa CFS peak values. Notice that longer period waves have significantly larger SSE triggering potential, i.e. ~40% larger final slip and much larger (effective) slip acceleration.